



CHICAGO JOURNALS



The University of Chicago

Warning Signals of Regime Shifts as Intrinsic Properties of Endogenous Dynamics.

Author(s): Tak Fung, Robert M. Seymour, and Craig R. Johnson

Source: *The American Naturalist*, Vol. 182, No. 2 (August 2013), pp. 208-222

Published by: [The University of Chicago Press](#) for [The American Society of Naturalists](#)

Stable URL: <http://www.jstor.org/stable/10.1086/670930>

Accessed: 15/07/2013 16:45

Your use of the JSTOR archive indicates your acceptance of the Terms & Conditions of Use, available at <http://www.jstor.org/page/info/about/policies/terms.jsp>

JSTOR is a not-for-profit service that helps scholars, researchers, and students discover, use, and build upon a wide range of content in a trusted digital archive. We use information technology and tools to increase productivity and facilitate new forms of scholarship. For more information about JSTOR, please contact support@jstor.org.



The University of Chicago Press, The American Society of Naturalists, The University of Chicago are collaborating with JSTOR to digitize, preserve and extend access to *The American Naturalist*.

<http://www.jstor.org>

Warning Signals of Regime Shifts as Intrinsic Properties of Endogenous Dynamics*

Tak Fung,^{1,†} Robert M. Seymour,^{2,3} and Craig R. Johnson⁴

1. Queen's University Belfast, School of Biological Sciences, 97 Lisburn Road, Belfast BT9 7BL, United Kingdom; 2. University College London, Centre for Mathematics and Physics in the Life Sciences and Experimental Biology, Gower Street, London WC1E 6BT, United Kingdom; 3. University College London, Department of Mathematics, Gower Street, London WC1E 6BT, United Kingdom; 4. University of Tasmania, Institute for Marine and Antarctic Studies, Private Bag 129, Hobart, Tasmania 7001, Australia

Submitted September 2, 2012; Accepted March 22, 2013; Electronically published June 28, 2013

Online enhancements: appendices.

ABSTRACT: Ecosystem dynamics can exhibit large, nonlinear changes after small changes in an environmental parameter that passes a critical threshold. These regime shifts are often associated with loss of biodiversity and ecosystem services. Because critical thresholds for regime shifts are hard to determine with precision, some recent studies have focused on deriving signals from dynamics leading up to the thresholds. Models in these studies depend on using noise terms independent of system parameters and variables to add stochasticity. However, demographic stochasticity, an important source of random variability, arises directly from system dynamics. In this study, a framework is developed for modeling demographic stochasticity in a mechanistic way, incorporating system variables and parameters. This framework is applied to a deterministic, dynamic model of a coral reef benthos. The resulting stochastic model indicates that increasing variance—but not skewness—is consistently found in system dynamics approaching a critical threshold of grazing pressure. Even if the threshold is breached, attraction of transient dynamics by a saddle point provides an opportunity for regime shift reversal by management intervention. These results suggest that early warning signals of regime shifts can arise intrinsically in endogenous dynamics and can be detected without reliance on random environmental forcings.

Keywords: coral reefs, demographic stochasticity, early warning signals, Markov process.

Introduction

There is clear evidence that a diversity of ecosystem types can demonstrate sudden, nonlinear changes beyond a critical parameter threshold, otherwise known as regime or phase shifts (Scheffer et al. 2001; Scheffer and Carpenter 2003; Folke et al. 2004). Regime shifts have been docu-

mented in both terrestrial and aquatic ecosystems, including savannas, lakes, kelp forests, and coral reefs (Holling 1973; Hughes 1994; Scheffer et al. 2001; Konar and Estes 2003; Folke et al. 2004; Ling et al. 2009). They often lead to decreased levels of biodiversity and ecosystem services (Folke et al. 2004), and so natural resource managers usually want to protect against their eventuality. Where ecosystems manifest alternative stable states (Scheffer et al. 2001; Petraitis and Dudgeon 2004; Schröder et al. 2005; Marzloff et al. 2011), not only is there a discontinuous change in equilibrium state at the critical threshold, typically corresponding to a saddle-node bifurcation (Guckenheimer and Holmes 1997), but system recovery is also hindered by hysteresis (Beisner et al. 2003; Carpenter and Brock 2006; Mumby et al. 2007). Thus, discontinuous regime shifts with hysteresis are particularly problematic for management.

A prominent aspect of the problem of avoiding regime shifts in natural systems, using appropriate management responses, is the difficulty of pinpointing the thresholds at which they occur. Although empirical evidence (Scheffer et al. 2001; Scheffer and Carpenter 2003; Hirota et al. 2011) and theoretical models (e.g., May 1977; Nakajima and DeAngelis 1989; Knowlton 1992) can provide insight into the ecological mechanisms giving rise to critical thresholds and a general indication of where thresholds may occur, it is difficult to determine precisely where thresholds occur without historical cases and/or direct experimentation, because the state of an ecosystem changes relatively slowly leading up to a regime shift (Scheffer and Carpenter 2003). Thus, regime shifts are typically observed only after the fact. However, there is mounting evidence that simulation models can help to identify thresholds with greater precision than previously thought (Marzloff et al. 2013).

In response to the challenge of preventing regime shifts, an expanding and promising area of research has focused on identifying early warning signals in system dynamics

* This paper is dedicated to the memory of Professor Robert M. Seymour, an inspired and inspiring mathematician, teacher, colleague, and friend.

† Corresponding author; e-mail: tfung01@qub.ac.uk.

Am. Nat. 2013. Vol. 182, pp. 208–222. © 2013 by The University of Chicago. 0003-0147/2013/18202-54091\$15.00. All rights reserved.

DOI: 10.1086/670930

leading up to a threshold (Scheffer et al. 2009). Theoretical modeling and, increasingly, empirical time series analyses and experiments have identified a number of warning signals in the dynamics of system variables that can be measured readily in the field, such as nutrient concentration, population abundance, and temperature. These signals include increasing standard deviation (SD) or variance (Brock and Carpenter 2006; Carpenter and Brock 2006, 2011; Biggs et al. 2009; Takimoto 2009; Carpenter et al. 2011; Dai et al. 2012), increasing skewness (Carpenter and Brock 2006; Guttal and Jayaprakash 2008; Drake and Griffen 2010), decreasing rate of return to equilibrium (van Nes and Scheffer 2007; Chisholm and Filotas 2009; Dai et al. 2012; Veraart et al. 2012), increasing autocorrelation (Dakos et al. 2008, 2012; Biggs et al. 2009; Drake and Griffen 2010), and a shift in the frequency spectrum to lower frequencies (Kleinen et al. 2003; Carpenter et al. 2008). Importantly, these signals are all premised on the existence of some type of stochasticity in the system and, apart from increasing skewness, depend on critical slowing down of system dynamics as the threshold is approached (Scheffer et al. 2009). This critical slowing down phenomenon is predicted from local equilibrium theory: close to a local equilibrium, it can be proved that in the long term, the rate of return to the local equilibrium approaches 0 as a bifurcation point is approached (Wissel 1984; Guckenheimer and Holmes 1997). Increasing skewness in the dynamics of variables in a system, on the other hand, has been hypothesized to result from another mechanism. As a saddle-node bifurcation point is approached, an unstable equilibrium gets closer to a stable equilibrium, such that for each system variable, an unstable equilibrium value gets closer to the stable equilibrium value from one side. This could lead to increasing effects of the unstable equilibrium on dynamics on one side of the stable equilibrium, resulting in increasing skewness (Scheffer et al. 2009).

Existing models used in studies of early warning signals, in systems with the capacity for regime shifts, typically introduce stochasticity by adding separate random noise terms to equations describing deterministic dynamics (Brock and Carpenter 2006; Carpenter and Brock 2006; Carpenter et al. 2008; Dakos et al. 2008, 2012; Guttal and Jayaprakash 2008; Biggs et al. 2009; Contamin and Ellison 2009; Takimoto 2009). Although this is an established method of generating stochasticity (e.g., Øksendal 1995; Mikosch 1998), noise is added by randomly sampling from distributions that are independent of system parameters and variables. Thus, the method is not well suited for representing demographic stochasticity, which is caused by and hence mechanistically linked to system dynamics (Schaffer 1981; Lande 1993; Bjørnstad and Grenfell 2001) and which may be an important source of random dynamical fluctuations (Bjørnstad and Grenfell 2001). De-

mographic stochasticity is the random variation that arises from a finite number of interacting units taking part in probabilistic interactions, in the absence of environmental variability (Bjørnstad and Grenfell 2001). In this article, we develop a mathematical framework that permits modeling of ecosystem dynamics with demographic stochasticity that is explicitly related to system parameters and variables, taking into account the system's carrying capacity. Thus, the source of stochasticity in this framework can be unambiguously attributed to endogenous dynamics (Hastings 2010), in the sense that it does not arise from exogenous environmental forcings, and can be considered intrinsic to the system.

To test whether early warning signals of regime shifts can be detected under the framework we develop, we apply the framework to a model of coral reef benthic systems (Fung et al. 2011); such systems are capable of exhibiting coral-algal regime shifts under increasing fishing pressure (e.g., Hughes 1994). This allows assessment of the degree to which these signals are an intrinsic, fundamental property of ecosystems. Specifically, we test for increasing variance and skewness in the dynamics of different coral reef benthic functional groups under different rates of approach to a critical fishing pressure threshold. Variance is examined owing to its ease of measurement for a variety of ecosystems (Brock and Carpenter 2010) and because it is predicted to increase approaching a critical threshold, as a result of critical slowing down (explained above; Scheffer et al. 2009). In particular, we determine whether transient short-term behavior can cause deviations from expected long-term trends predicted by critical slowing down (Neubert and Caswell 1997). Trends in the coefficient of variation (SD divided by the mean) are not examined in this article because it is a priori unclear how the predicted increasing trends in SD would be affected by dividing by the means, which also change leading up to a critical threshold. Increasing skewness is examined because it is a commonly proposed early warning signal based on reasoning that does not depend on critical slowing down (Scheffer et al. 2009). Furthermore, we examine dynamics after a critical threshold has been crossed to see whether there is a transient state before the new equilibrium is reached. Such a transient state may arise because of attraction of dynamics by an unstable saddle point (Hastings 2004) and could signal to managers a last opportunity for prevention of a regime shift. We conclude with a discussion of the theoretical and practical implications of our results in relation to existing research on early warning signals of regime shifts and future perspectives that include incorporating spatial structure and environmental stochasticity into our framework. Our study is the first to focus on the effects of demographic stochasticity on the detection of early warning signals and is a first examination of whether

these signals can be detected for regime shifts in coral reef ecosystems.

Methods

Introducing Demographic Stochasticity Using a Markov Process

Demographic stochasticity is the random variation that results from a finite number N of discrete ecosystem units partaking in ecological processes with given probabilities, in the absence of changes in system parameters and variables caused by environmental variability (Schaffer 1981; Lande 1993; Bjørnstad and Grenfell 2001). A unit could be an individual or—for sessile organisms, such as grass or corals—a colony or an area of fixed size. Each of the N units is in a particular state; for an individual, the states could be “alive” or “dead,” whereas for an area of fixed size, the states could be “occupied by a particular type of organism” or “unoccupied.” If there are $x + 1$ states ($x \geq 1$), then there is a state vector $\mathbf{S} = \{0, 1, \dots, x\}$ and a corresponding system state vector $\mathbf{N} = \{N_0, N_1, \dots, N_x\}$, the elements of which are the number of units in state i . In each time step considered, an $x + 1$ by $x + 1$ transition matrix $\mathbf{P} = (p_{ij})$ can be defined, with entries p_{ij} equal to the probability of a unit in state i being in state j in the next time step. These probabilities are a function of the ecosystem parameters, which are fixed, and variables. Because N is finite, stochasticity arises from the probabilistic determination of the state of each unit in consecutive time steps.

A Markov process approach to modeling demographic stochasticity has been used in previous studies of the dynamics of single-species populations (e.g., Schaffer 1983; Akçakaya 1991; Gilpin 1992; Caswell 2001). More broadly, Markov processes have been used to add stochastic variation to dynamics of model metabolic pathways (e.g., Kelsey et al. 2008) and, in population genetic models, to represent changes in allelic frequencies due to random sampling of mating individuals in a finite population (e.g., Maynard Smith and Haigh 1974; Hartl and Clark 1997). Markov models have also been used to describe the dynamics of sessile communities, although they rarely consider density dependence (Spencer and Tanner 2008).

Our study builds on this previous work by developing a framework, using a Markov process approach, for introducing demographic stochasticity to a set of deterministic differential equations, which is sufficiently flexible to accommodate interspecific interactions represented by complex, nonlinear terms that may be density dependent. These interactions are more complex than those found in Lotka-Volterra models (e.g., MacArthur and Levins 1967; Spencer and Tanner 2008). To clearly illustrate how the

framework operates, it is applied to a model of a coral reef benthos, but the framework can be applied to other similar models in the same way.

Stochasticizing a Coral Reef Benthic Model

The Coral-Turf-Macroalgae model (CTMm) of Fung et al. (2011) is considered, which models the deterministic dynamics of three main functional groups—hard corals, turf algae, and macroalgae—competing for space on a coral reef benthos at a local scale smaller than the order of tens of kilometers. Each group is defined by its proportional cover, which changes dynamically according to the set of ordinary differential equations:

$$\begin{aligned} \frac{dC}{dt} = & \underbrace{(l_c^s + l_c^b C)(S + \varepsilon_c T)}_{\text{coral recruitment}} \\ & + \underbrace{r_C(1 - \beta_M M)(S + \alpha_c T)C}_{\text{coral growth}} \\ & - \underbrace{d_C C}_{\text{coral mortality}} \\ & - \underbrace{\gamma_{CM} r_M MC}_{\text{macroalgal growth over corals}}, \end{aligned} \quad (1)$$

$$\begin{aligned} \frac{dT}{dt} = & \underbrace{\zeta_T(1 - \theta)S}_{\text{turf algal growth}} - \underbrace{g_T \theta T}_{\text{grazing on turf}} \\ & - \underbrace{\varepsilon_c l_c^s + l_c^b C}_{\text{coral recruitment on turf}} T \\ & - \underbrace{\alpha_c r_C(1 - \beta_M M)TC}_{\text{coral growth over turf}} \\ & - \underbrace{\gamma_{TM} r_M MT}_{\text{macroalgal growth over turf}}, \end{aligned} \quad (2)$$

$$\begin{aligned} \frac{dM}{dt} = & \underbrace{r_M M(S + \gamma_{CM} C + \gamma_{TM} T)}_{\text{macroalgal growth}} \\ & - \underbrace{g_M \theta M}_{\text{grazing on macroalgae}}. \end{aligned} \quad (3)$$

Here, C , T , and M are the proportional covers of hard corals, turf algae, and macroalgae, respectively. The cover of space—which is the area of the modeled benthos not covered by corals, turf algae, or macroalgae—is simply $S = 1 - C - T - M$. A full justification of the interactions modeled is given by Fung et al. (2011); table 1 gives a list of the parameters in the model.

Following a Markov process approach to introducing demographic stochasticity, the benthic area is first conceptualized as N discrete interacting units of equal size.

Table 1: Parameter definitions for the Coral-Turf-Macroalgae model (CTMm), specified by equations (1)–(3)

Parameter	Definition
θ	Grazing pressure
d_C	Coral mortality rate
l_C^b	Rate at which coral larvae, produced by local established brooding corals, recruit onto space
l_C^s	Rate at which exogenous spawning coral larvae recruit onto space
r_C	Lateral growth rate of corals over space
α_C	Growth rate of corals over turf, relative to the rate over space
ε_C	Recruitment rate of corals onto turf, relative to the rate onto space
g_T	Maximum rate at which turf algae is grazed
ζ_T	Growth rate of fine turf (occupying space)
g_M	Maximum rate at which macroalgae is grazed
r_M	Lateral growth rate of macroalgae over space
β_M	Coral growth is inhibited by the presence of nearby macroalgae, and this is represented as depression of r_C by the factor $(1 - \beta_M M)$, where M is the macroalgal cover
γ_{CM}	Lateral growth rate of macroalgae over corals, relative to the rate over space
γ_{TM}	Lateral growth rate of macroalgae over turf, relative to the rate over space

Each of these units can be occupied by corals, turf algae, or macroalgae or left unoccupied by these previous groups. Hence, there are four states indexed by $\mathbf{S} = \{0, 1, 2, 3\}$, with the corresponding system state vector being $\mathbf{N} = \{N_0, N_1, N_2, N_3\}$. N_0 , N_1 , and N_2 are the number of units occupied by corals, turf algae, and macroalgae, respectively, and N_3 is the number of units of space. The proportional covers are thus defined by $C = N_0/N$, $T = N_1/N$, $M = N_2/N$, and $S = N_3/N$. The Markov process approach works in discrete time, so the differential equations (1)–

(3) are converted to the corresponding difference equations using a small, fixed time interval δt . For each discrete time step, the probabilities in the transition matrix $\mathbf{P} = (p_{ij})$ can be derived by noting that the rates of ecological processes in equations (1)–(3), when multiplied by δt , can be interpreted as the probabilities of those processes occurring in δt . A formal mathematical method for defining p_{ij} is given in appendix A (apps. A–E are available online), which also affirms that the probabilities derived define a Markov process. This method gives the transition matrix

$$\left(\begin{array}{c|cccc} & C & T & M & S \\ \hline C & 1 - g_{CM} - m_{CS} & 0 & g_{CM} & m_{CS} \\ T & g_{TC} + r_{TC} & 1 - g_{TC} - g_{TM} - m_{TS} - r_{TC} & g_{TM} & m_{TS} \\ M & 0 & 0 & 1 - m_{MS} & m_{MS} \\ S & g_{SC} + r_{SC} & g_{ST} & g_{SM} & 1 - g_{SC} - g_{SM} - g_{ST} - r_{SC} \end{array} \right), \quad (4)$$

where

$$g_{CM} = \gamma_{CM} r_M M \delta t, \quad (5a)$$

$$g_{TC} = \alpha_C r_C (1 - \beta_M M) C \delta t, \quad (5b)$$

$$g_{TM} = \gamma_{TM} r_M M \delta t, \quad (5c)$$

$$g_{SC} = r_C (1 - \beta_M M) C \delta t, \quad (5d)$$

$$g_{ST} = \zeta_T (1 - \theta) \delta t, \quad (5e)$$

$$g_{SM} = r_M M \delta t, \quad (5f)$$

$$m_{CS} = d_C \delta t, \quad (5g)$$

$$m_{TS} = g_T \theta \delta t, \quad (5h)$$

$$m_{MS} = g_M \theta \delta t, \quad (5i)$$

$$r_{TC} = (\varepsilon_C l_C^s + \varepsilon_C l_C^b C) \delta t, \quad (5j)$$

$$r_{SC} = (l_C^s + l_C^b C) \delta t. \quad (5k)$$

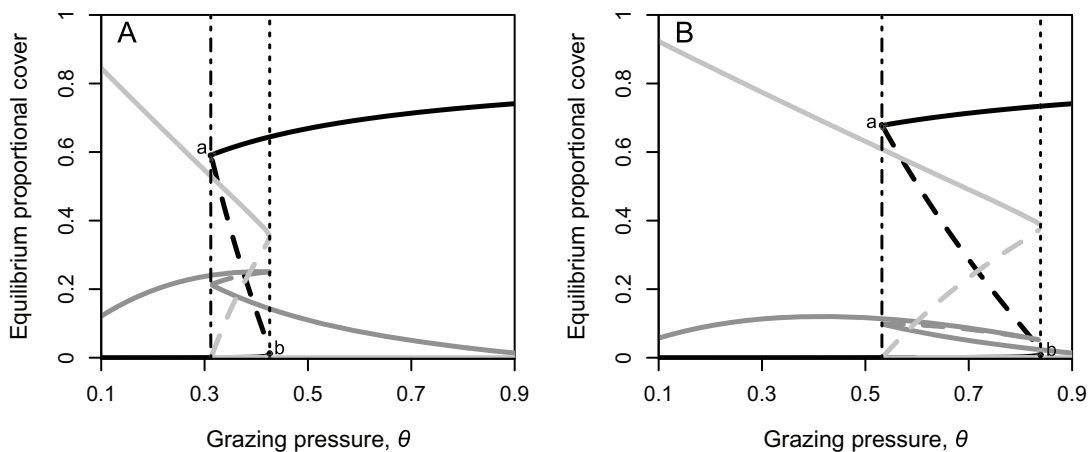


Figure 1: Phase diagrams showing equilibria for the deterministic coral reef benthic model specified by equations (1)–(3) as the grazing pressure parameter θ is changed between 0.1 and 0.9. Black, dark gray, and light gray lines are the equilibrium proportional covers of corals, turf algae, and macroalgae, respectively; solid and dashed lines refer to stable and unstable equilibria, respectively. The dashed and dotted vertical line marks a transcritical bifurcation, whereas the dotted vertical line marks a saddle-node bifurcation; a and b represent bifurcation points for coral cover. A, Parameter set used is the same as that used by Fung et al. (2011) for their figure 3C. B, Parameter set used is the same as for A, except that the macroalgal growth rate r_M is doubled to 0.7 year^{-1} .

It can be proved that the expected dynamics of this stochastic version of the model closely approximates dynamics given by equations (1)–(3) (app. A). This provides a logical interpretation of the deterministic model as the limit reached by the stochastic model as $N \rightarrow \infty$; in this limit of infinite system size, demographic stochasticity becomes 0.

A time step of $\delta t = 1$ day is used in this study, whereas the size of a discrete benthic unit is chosen by considering the typical area taken up by components of the functional groups modeled. Coral colonies typically have an area on the order of 0.01 m^2 , based on the median of 29 mean radii values from 25 coral populations in the western Atlantic (García-Salgado et al. 2006) and four coral populations in the Indo-Pacific (Sandin et al. 2008). In addition, at two reefs in Belize, patches of the macroalga *Dictyota pulchella* have mean areas on the order of 0.01 m^2 (Mumby et al. 2005). Thus, in our model, one discrete unit is taken to represent 0.01 m^2 . The total number of units modeled, N , is taken to be 1,000; to test sensitivity of results to N , simulations with 10,000 units are also performed. Thus, model runs correspond to reef areas on the order of 10–100 m^2 . This is the typical scale at which coral reef benthic cover is surveyed using transects, which typically have a length of a few tens of meters and a width of 0 (line intercept transects) or tens of centimeters to meters (belt transects; Hill and Wilkinson 2004; García-Salgado et al. 2006).

Detection of Warning Signals in Stochastic Model

To test for warning signals preceding a regime shift, a set of parameters is chosen that gives a bifurcation with increasing fishing pressure or, equivalently, decreasing grazing pressure on algae (θ) for the deterministic model. This parameter set is the same as that used to produce figure 3C of Fung et al. (2011) and is reproduced in appendix B; the corresponding phase diagram is shown in figure 1A. As θ decreases from a high value of 0.9 (high grazing, low fishing), the system crosses a region with alternative stable states and approaches a critical threshold of $\theta_c^- = 0.312$, which is determined numerically (fig. 1A). At this threshold, there is a transcritical bifurcation between two equilibria with high coral cover, which exchange stability (i.e., one stable equilibrium becomes unstable and one unstable equilibrium becomes stable; point a in fig. 1A). The stable equilibrium that results from this bifurcation has negative macroalgal cover, so the resulting system is left with only one stable equilibrium within the biological domain, with low coral and high algal (turf algal plus macroalgal) cover (fig. 1A). The reverse situation occurs when θ increases from a low value of 0.1. In this case, the system undergoes a saddle-node bifurcation at the critical threshold of $\theta_c^+ = 0.426$, which is again determined numerically; for coral cover, the bifurcation point is marked as b in figure 1A. Thereafter, the system has only one stable equilibrium, with high coral and low algal cover (fig. 1A).

First, the SD and skewness of dynamics given by the

stochastic version of the model are calculated for values of θ decreasing from 0.9 to 0.1 in increments of 0.025. At each value of θ , the stochastic model is run for 2,000 years, which is more than enough time to guarantee convergence to a stationary state. For each $\theta > \theta_c^- = 0.312$, initial proportional covers are chosen that allow the system to converge to the stationary state with high (>0.5) mean C (corresponding to the equilibrium with high C in the deterministic model); the initial values of C , T , and M used are 0.6, 0.1, and 0.1, respectively, or 0.8, 0.1, and 0.05. For each $\theta < \theta_c^- = 0.312$, initial values of 0.1, 0.1, and 0.6, respectively, are used, allowing the system to converge quickly to the stationary state with low (<0.5) mean C . For each 2,000-year simulation, data points for the past 1,500 years are taken to define stationary distributions for C , T , and M , since in all runs, convergence has occurred within 500 years (determined by visual inspection; for graphical examples, see app. B). The SD and skewness for each of the three distributions are then calculated. These simulations model the situation where fishing decreases θ very slowly, such that stationary dynamics are approximated. Graphs of SD and skewness against θ are plotted to see whether there are any trends leading up to the critical value of $\theta_c^- = 0.312$, determined from the deterministic model as described above. Simulations are also performed for the opposite case of increasing θ —from 0.1 to 0.9—to see whether there are any trends leading up to the critical value of $\theta_c^+ = 0.426$, determined from the deterministic model. This examines whether dynamics exhibit “warning” signals of system recovery. In this case, SD and skewness for $\theta < \theta_c^- = 0.312$ and $\theta > \theta_c^+ = 0.426$ are the same as in the case of decreasing θ , since dynamics converge to only one stationary state at each θ . Thus, SD and skewness values are taken directly from the previous case. However, for each $0.312 < \theta < 0.426$, initial covers are chosen that allow the system to converge to the stationary state with low mean C ; that is, initial values of C , T , and M are chosen to be 0.1, 0.1, and 0.6, respectively, or 0.05, 0.1, and 0.8. To determine whether the trends in SD and skewness found depend on the location of the critical thresholds—that is, the values of θ_c^- and θ_c^+ —the exercise described in this paragraph is repeated for the same set of parameters but with the macroalgal growth rate r_M doubled (all parameter values are given in app. B), which gives $\theta_c^- = 0.532$ and $\theta_c^+ = 0.839$ (fig. 1B).

Second, SDs of C , T , and M are calculated as θ is changed continuously through time. Skewness is not considered because from the first part of the analysis, described in the previous paragraph, trends in SD are much more consistent than trends in skewness approaching a critical threshold. In addition, the first part of the analysis showed that results using 10,000 units in simulations gave the same trends as those using 1,000 units and that increasing r_M

and hence θ_c^- and θ_c^+ , gave largely the same trends. Thus, for further analyses, only 1,000 units and the original parameter set are used. Continuously changing θ represents scenarios where fishing pressure changes quickly enough such that dynamics do not have time to approximate a stationary state. A key theoretical and practical question here is: can early warning signals still be detected? To examine this for the case of increasing fishing pressure, dynamics are first run for 100 years with high $\theta = 0.9$, starting at the equilibrium values for the corresponding deterministic model; this allows the system to stabilize at high coral and low algal cover. θ is then continuously decreased to 0.3, just beyond the critical value of 0.312, over the course of 400 years, representing a slow rate of decrease. During this period, SDs over time are calculated using cover values within a time window of fixed length that moves forward continuously in time; at a given time t , SDs for C , T , and M are calculated using cover values within the window that ends at t . For these sliding windows, lengths of 5, 10, 25, 50, and 100 years are tested. This exercise is repeated 10,000 times, allowing the means and standard errors of the SDs to be calculated. Four quicker rates of decrease of θ are also investigated, from $\theta = 0.9$ to 0.3 in 200, 100, 50, and 25 years.

For each rate of decrease of θ , the sliding window length giving SD values for C at $\theta = 0.9$ and 0.3 that best match corresponding values for the stationary distributions is calculated to derive the optimum sliding window length that best captures the increase in SD due to increasing proximity of the critical threshold. The match is measured by the average absolute percentage difference for the two pairs of SD values at $\theta = 0.9$ and 0.3. For the optimum window length found, the SD trend for C is recalculated using annual samples, reflecting a realistic surveillance scenario (e.g., for the Great Barrier Reef; <http://www.aims.gov.au/docs/research/monitoring/reef/reef-monitoring.html>). To investigate the effects of coarser sampling, SD trends using samples every 2 and 3 years are also calculated. In addition, for annual sampling, once θ decreases past 0.65 at time $t_{\theta=0.65}$, the lag in detecting the corresponding increase in SD for C is calculated as the time at which the optimum sliding window length first gives an SD greater than or equal to the SD for the stationary distribution of C at $\theta = 0.65$ minus $t_{\theta=0.65}$. Lags are also calculated for $\theta = 0.55, 0.45, \text{ and } 0.35$. The lag times measure the power of realistic surveillance regimes to detect changes in SD for C when approaching a critical threshold. Calculations in this paragraph are repeated for the SD values for T .

Third, simulations are run to test the hypothesis that an unstable saddle point can give rise to a transient state in dynamics after θ crosses the critical value, by temporarily attracting dynamics (Hastings 2004). Such an un-

stable ghost attractor (Strogatz 1994) could cause dynamics to fluctuate temporarily around its associated equilibrium values, giving a characteristic warning signal during a regime shift. To test the hypothesis, a simulation is run with high $\theta = 0.7$ for 1,000 years, with initial values of 0.6, 0.1, and 0.1 for coral, turf algal, and macroalgal cover, respectively. This ensures that the system reaches a stationary state with high coral and low algal cover; in fact, macroalgal cover is zero. Then, θ is decreased to 0.3, just beyond the critical value of 0.312. This models a strong increase in fishing pressure on herbivores (herbivorous fish and sea urchins) over a short period of time or, alternatively, a sharp decrease in θ brought about by mass mortality of herbivores, such as the disease-induced mass mortality of *Diadema antillarum* urchins on Caribbean coral reefs in 1983–1984 (Lessios 1988). At the same time, macroalgal cover is increased by 0.01, representing a small recruitment of macroalgal propagules from outside the modeled area (Kinlan et al. 2005). This is necessary for initiating a regime shift to a stationary state with low coral cover, because this state also has nonzero macroalgal cover, and the only way for the system to move from a state with zero macroalgal cover to a state with nonzero macroalgal cover is if there is some exogenous macroalgal recruitment (see probability transition matrix [4]). Dynamics are tracked for a further 1,000 years to determine whether a warning signal is evident during the regime shift; 1,000 years is more than enough time to guarantee that the regime shift has occurred. This simulation is repeated a further nine times to assess whether the period of attraction by the saddle point varies stochastically.

The stochastic model was implemented using C++ code, and this implementation was used to perform all stochastic simulations.

Results

Trends in SD and Skewness for Stationary Dynamics

For each type of proportional cover, stochastic model runs produced stationary distributions with mean values very close to deterministic values in the phase diagrams in figure 1. The correlation was high ($r^2 > 0.998$; $n = 38$ and 45 for phase diagrams in fig. 1A and 1B, respectively), and the regression lines had y -intercepts close to 0 (magnitude < 0.001) and slopes close to 1 (< 0.001 away from 1). This is the case using 1,000 or 10,000 discrete benthic units, and it shows that critical θ values for the deterministic model can be used as critical values for the stochastic model as well.

For 1,000 units and the original set of parameters (without increased r_M), as $\theta \rightarrow \theta_c^- = 0.312$ from an initial value of 0.9, SD for stationary dynamics of C and T both showed

an increasing trend (fig. 2A); the overall increases in SD of C and T as grazing pressure decreased from $\theta = 0.9$ to 0.325 were 26% and 311%, respectively. M remained at 0 before the critical threshold; hence, its SD remained at 0 too. Skewness for C fluctuated wildly with no clear trend, whereas that for T displayed a decreasing trend, with an overall decrease of 95% (fig. 2B). For the opposite scenario of increasing θ , where $\theta \rightarrow \theta_c^+ = 0.426$ from an initial value of 0.1, SD for stationary dynamics of C , T , and M all showed increasing trends (fig. 2C), with overall increases from $\theta = 0.1$ to 0.425 of 3,188%, 40%, and 87%, respectively. Although the percentage increase in C is very large, it corresponds to a low absolute increase from 0.000301 to 0.00989. Skewness for C remained very high (> 1) as the threshold is approached, whereas that for T and M did not exhibit any clear trends, with large fluctuations for M (fig. 2D). The very high skewness of C reflects low values of C , which had a mean of < 0.01 before the threshold.

For the set of parameters with increased r_M , trends in SD and skewness approaching a critical parameter threshold were largely the same as that found for the original parameter set. The only qualitative difference was seen in the case of increasing θ ; as $\theta \rightarrow \theta_c^+ = 0.839$ from a starting value of 0.1, SD for T showed an increasing trend up to $\theta = 0.425$ but thereafter showed a decreasing trend up to $\theta = 0.825$. Appendix C presents a detailed mathematical analysis of dynamics for T at these two θ values, demonstrating that the decrease in SD could have arisen from stochastic fluctuations of T that were frequent enough to cause deterministic dynamics in between fluctuations to deviate from long-term trends.

Using 10,000 units instead of 1,000, the same trends for SD and skewness were found for the different proportional covers. This was in spite of decreased stochasticity resulting in decreased SD values. Appendix D shows results for 10,000 units corresponding to figure 2.

Trends in SD for Continuously Changing θ

For simulations where θ is continuously decreased from 0.9 to 0.3 over 400, 200, 100, 50, or 25 years, the mean SDs for all proportional covers over 10,000 independent runs were tracked through time for sliding window lengths of 5, 10, 25, 50, and 100 years. In all of these simulations, the initial value of M was 0; hence, M remained at 0 throughout (see probability transition matrix [4]). For C and T , the standard error of the SD at any point in time in any of the simulations was always small relative to the mean ($< 0.44\%$), indicating low uncertainty for the mean SD values found.

The mean SD for coral cover (C) showed a flat or slightly decreasing trend over time for a window length of 5 years,

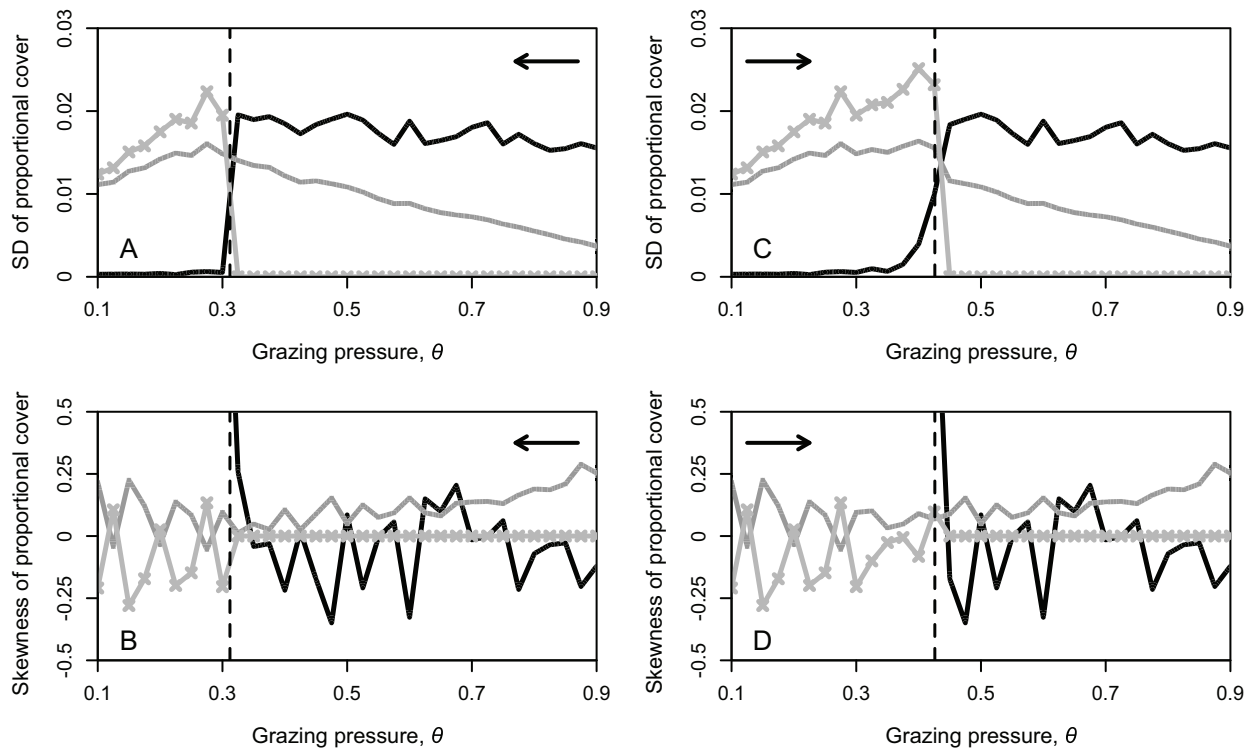


Figure 2: A, B, For the stochastic coral reef benthic model with 1,000 discrete units, trends in standard deviation (SD) and skewness of stationary distributions of model variables as the grazing pressure θ decreases from 0.9 to 0.1 in increments of 0.025. Black, dark gray, and light gray lines correspond to the proportional covers of corals, turf algae, and macroalgae, respectively. Crosses on the light gray lines indicate the values of θ simulated. For macroalgal cover, skewness is set to 0 if the mean is 0. The dashed vertical lines represent the critical θ value, whereas arrows indicate the direction of changing θ . The parameter set used is the same as that used to draw the phase diagram in figure 1A. C, D, Same as A and B, respectively, except for the case where θ increases from 0.1 to 0.9.

except when θ decreased quickly over ≤ 50 years, and for a window length of 10 years, except when θ decreased sufficiently quickly over ≤ 100 years (fig. 3A). For other combinations of window length and rate of θ decrease, the mean SD increased after a delay of typically more than 15 years (fig. 3A). For long window lengths of ≥ 50 years in scenarios where θ decreased over ≤ 200 years, and for the longest window length of 100 years when θ decreased over 400 years, mean SD eventually exceeded the maximum SD of about 0.02 for the stationary distributions (fig. 3A). The increase in mean SD typically increased with window length (fig. 3A). In contrast, mean SD for T showed an increasing trend sooner than C for all window lengths (fig. 3B). For window lengths ≥ 25 years, regardless of the rate at which θ decreased, the mean SD was eventually close to or higher than the maximum SD of about 0.015 for the stationary distributions, sometimes reaching values more than three times as large (fig. 3B). As for C , the mean SD for T typically increased with window length (fig. 3B). For a fixed window length, the mean SD for C showed a

greater rate of change as the rate of decrease of θ increased (fig. 3C). This trend was repeated for T (fig. 3D).

The optimum sliding window length for the SD of C was always longer than that for the SD of T , regardless of the rate of decrease of θ (table 2). Considering both types of SD, the optimum window length typically decreased when θ decreased at a quicker rate (over fewer years). Using the optimum window lengths, trends for both types of SD calculated using annual sampling were always close to those using the entire data set. Considering all years from when θ started to decrease, the average absolute percentage difference was $<3\%$, except for the SD of T when θ decreased over 25 years, for which the difference was $<7\%$. For sampling every 2 years, the percentages were $<8\%$ and $<22\%$, respectively, whereas for sampling every 3 years, they were $<10\%$ and $<24\%$, respectively. For the case of annual sampling, lag times for detecting increases in the SD of C as predicted using stationary distributions of C (fig. 2A) were usually longer than those for detecting corresponding increases in the SD of T , sometimes by an

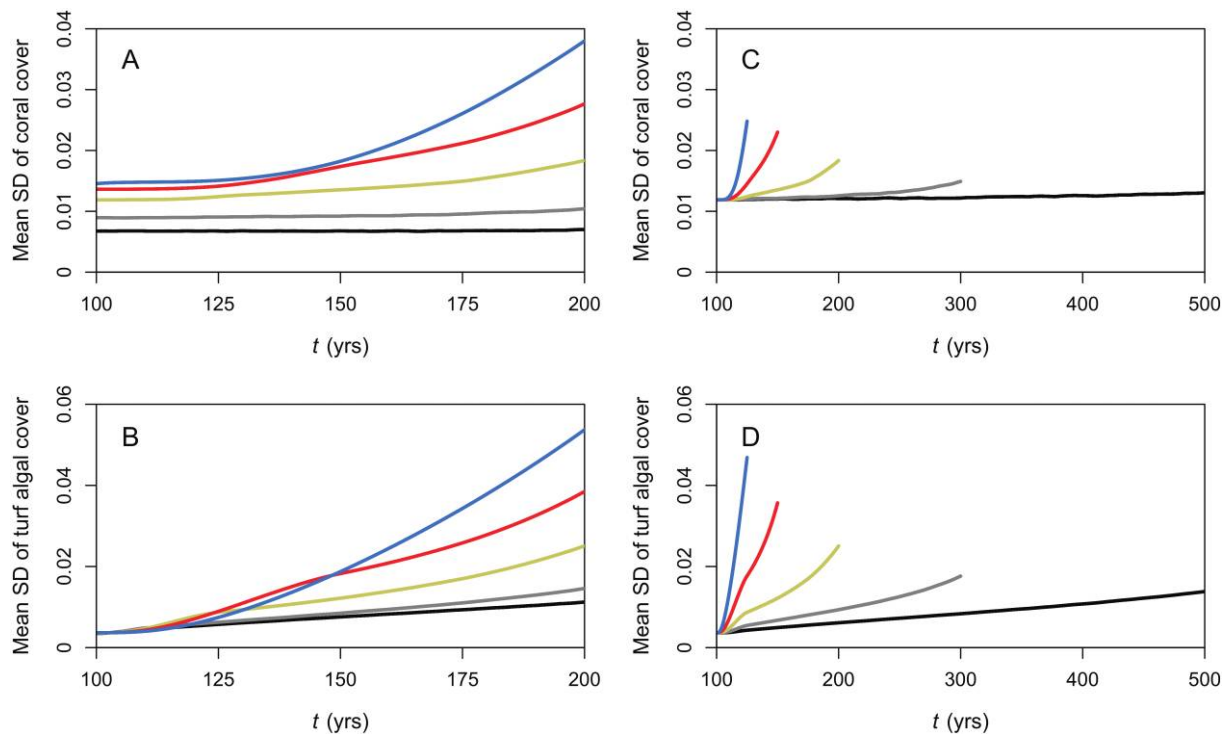


Figure 3: A, B, For the stochastic coral reef benthic model with 1,000 discrete units, trends in mean standard deviation (SD) for coral and turf algal covers, respectively, for the case where grazing pressure θ decreases from 0.9 to 0.3 over 100 years. The parameter set used is the same as that for figure 1A. Black, gray, yellow, red, and blue lines correspond to means from 10,000 runs of the stochastic coral reef benthic model for sliding windows of length 5, 10, 25, 50, and 100 years, respectively. For each run, dynamics were simulated for 100 years before θ was decreased to allow dynamics to stabilize. C, D, Trends in mean SD for coral and turf algal covers for a sliding window of length 25 years. Black, gray, yellow, red, and blue lines correspond to means from 10,000 stochastic model runs for the cases where θ decreases from 0.9 to 0.3 over 400, 200, 100, 50, and 25 years, respectively. Parameter values are the same as for A and B.

order of magnitude (table 2). Lags for the SD of T were typically <11 years (table 2). In about a quarter of cases, increases in SD were not detected (lag times of infinity), particularly when θ decreased sufficiently slowly over ≥ 100 years, or were detected before θ had reached the value considered (negative lag times), particularly when θ decreased quickly over ≤ 50 years (table 2). Infinite lag times reflect θ reaching 0.3 before the increase in SD considered can be detected, whereas negative lag times reflect additional SD caused by the moving average of the variables.

Warning Signals during a Regime Shift

Starting at a stationary state derived using the original set of parameter values with $\theta = 0.7$, decreasing θ to 0.3 while increasing M to 0.01 initiated a coral-algal regime shift (fig. 4A). Transient dynamics during this shift were attracted to the unstable saddle point that existed. This was manifested most clearly as a temporary period of stability at an intermediate value of coral cover sandwiched between two sharp drops in coral cover, the latter being much

greater than the first (fig. 4A). This simulation was repeated nine times with different seeds for the random number generator. It was found that the length of the temporary period of stability varied between runs as a result of stochasticity and can be longer or shorter than predicted by the deterministic dynamics, sometimes by more than 50 years (app. D).

The presence of an intermediate period of stability as fishing pressure is increased (grazing pressure is decreased) raises the question of whether the system can revert back to a healthy one with persistently high coral cover if fishing pressure is reduced (grazing pressure is increased) during this period. Thus, for the simulation shown in figure 4A, 100 years after grazing pressure θ is decreased to 0.3, it is increased to 0.35 again to see whether coral cover recovers, despite the system having crossed the critical value of θ at which it would tend toward an alternative stable state with low coral and high algal cover; 0.35 is just above the critical value of 0.312. This did cause the system to revert back to high coral cover, in effect reversing the course of the

Table 2: Optimum sliding window lengths and lag times for the standard deviations (SDs) of coral (*C*) and turf algal (*T*) covers

Time period of decreasing θ (years) and variable	Optimum sliding window length (years)	Lag for SD (years)			
		$\theta = 0.65$	$\theta = 0.55$	$\theta = 0.45$	$\theta = 0.35$
400:					
<i>C</i>	50	174.3	152.7	∞	∞
<i>T</i>	25	6.3	10.7	28.0	20.3
200:					
<i>C</i>	50	39.7	27.3	13.0	-11.3
<i>T</i>	10	14.7	23.3	39.0	∞
100:					
<i>C</i>	25	43.3	32.7	23.0	∞
<i>T</i>	10	.3	.7	4.0	.3
50:					
<i>C</i>	25	10.2	4.8	.5	-5.8
<i>T</i>	5	2.2	2.8	4.5	3.2
25:					
<i>C</i>	100	7.6	4.4	2.2	-.9
<i>T</i>	5	-3.4	-3.6	-3.8	-4.9

For the stochastic coral reef benthic model with the parameter set used to draw the phase diagram in figure 1A and 1,000 discrete units, optimum sliding window lengths and, under annual sampling, lag times for the SDs of coral and turf algal proportional covers for scenarios where grazing pressure θ decreases from 0.9 to 0.3 over different time periods. For definitions of the optimum sliding window length and the lag time at a particular θ value, see "Methods."

regime shift (fig. 4B). Appendix D shows another example of this reversal for the case of nutrient enrichment.

Discussion

Early warning signals of regime shifts in ecosystems provide an opportunity for managers to enact preventative measures to avert potentially large losses in biodiversity and ecosystem services (Scheffer et al. 2001, 2009; Scheffer and Carpenter 2003; Folke et al. 2004). Modeling studies (Wissel 1984; DeAngelis and Nakajima 1989; van Nes and Scheffer 2003; Rietkerk et al. 2004; Brock and Carpenter 2006, 2010; van Nes and Scheffer 2007; Carpenter et al. 2008; Guttal and Jayaprakash 2008; Biggs et al. 2009; Chisholm and Filotas 2009; Contamin and Ellison 2009; Takimoto 2009; Carpenter and Brock 2011; Dakos et al. 2011, 2012) allied with empirical time series analyses and experiments (Dakos et al. 2008; Carpenter et al. 2011; Dai et al. 2012) have provided evidence supporting the existence of early warning signals for a wide range of ecosystems.

However, thus far, studies have not focused on the way in which stochasticity is represented in models, which is typically added as noise terms independent of system parameters and variables. In this way, it is difficult to distinguish between demographic stochasticity, which is intrinsically linked to endogenous dynamics and hence to all system parameters and variables, and environmental

stochasticity, which arises from exogenous sources (Schaffer 1981; Lande 1993; Bjørnstad and Grenfell 2001; Hastings 2010). Furthermore, this approach assumes that noise acts directly on dynamic variables rather than the parameters. Dakos et al. (2012) address this issue by considering environmental stochasticity acting directly on parameters but not the problem of modeling demographic stochasticity, which may be an important source of dynamical fluctuations in ecosystems (Bjørnstad and Grenfell 2001).

A Markov Process Framework for Modeling Demographic Stochasticity

In this study, we have built on previous modeling studies of early warning signals by first constructing a general framework allowing demographic stochasticity to be added to deterministic dynamics, by relating it to all system parameters and variables in a Markov process. This framework thus gives a mechanistic relationship between the modeled stochasticity and endogenous dynamics. It can be applied to models of ecosystems with one or more groups that exhibit intra- and/or intergroup competition for a common resource, such as vegetation in arid ecosystems (Guttal and Jayaprakash 2008) and savannas (Hirota et al. 2011) or sessile organisms in rocky intertidal (Dayton 1971) and coral reef (Hughes 1994) ecosystems. Importantly, the form of the model need not be restricted

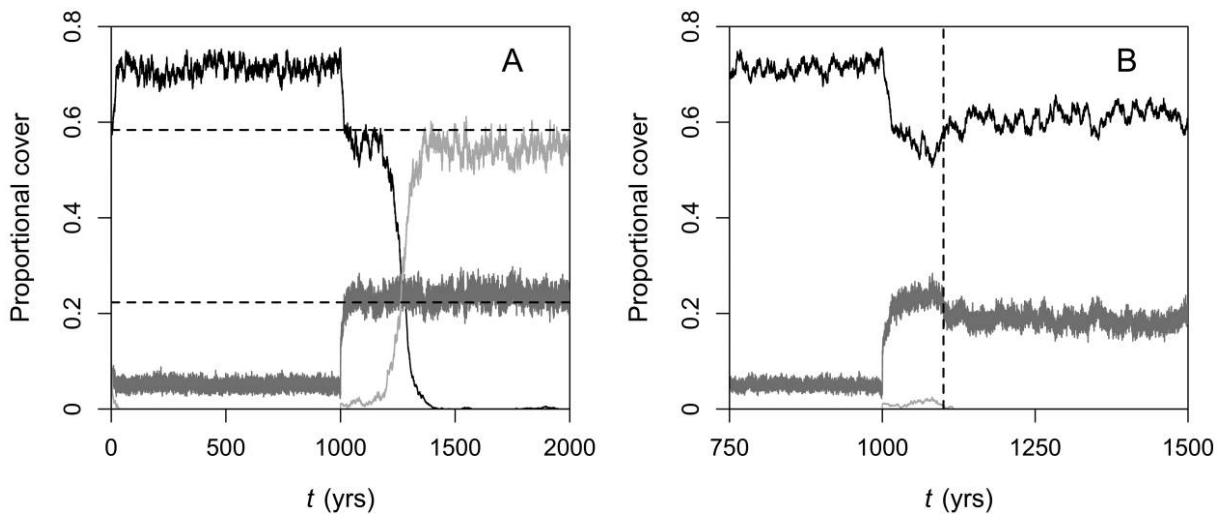


Figure 4: A, Stochastic coral reef benthic model run with the parameter set used to draw the phase diagram in figure 1A and grazing pressure parameter $\theta = 0.7$ for the first 1,000 years. One thousand discrete benthic units were used. Black, dark gray, and light gray lines correspond to coral, turf algal, and macroalgal covers, respectively; the initial values of these three types of cover are 0.6, 0.1, and 0.1, respectively. At 1,000 years, θ is decreased to 0.3, and macroalgal proportional cover is increased from 0 by 0.01 to simulate a macroalgal recruitment event. This initiates a regime shift to low coral cover. However, coral cover follows a stepwise decrease because of attraction to an unstable saddle point. The equilibrium coral and turf algal covers for this saddle point are marked by dashed horizontal lines; the equilibrium macroalgal cover is 0. B, Same as A, except that during the regime shift at 1,100 years (dashed vertical line), θ is increased to 0.35. This causes the regime shift to be reversed.

to Lotka-Volterra types (e.g., MacArthur and Levins 1967; Spencer and Tanner 2008).

Stochastic models that result from application of the framework can be used to assess whether early warning signals can exist in these ecosystems just from demographic stochasticity. This was demonstrated for a model of a coral reef benthos (Fung et al. 2011) under increasing fishing pressure (decreasing grazing pressure) and two commonly proposed signals, SD and skewness. Encouragingly from a management perspective, a trend of increasing SD was found for at least one variable as a critical threshold of grazing pressure was approached, independent of the threshold value and regardless of whether grazing pressure changed slowly or quickly (figs. 2, 3; app. C). In addition, increasing the spatial area by an order of magnitude for some simulations did not affect the trends found (fig. 2; app. D), suggesting that although demographic stochasticity decreases with system size, the trends are invariant. As for recovery rates to equilibrium following a small perturbation, relative rather than absolute rates seem to be more important (van Nes and Scheffer 2007). In addition, increasing SD was also found in the opposite direction of decreasing fishing pressure, which may be of use as a signal indicating reversal of a coral-algal regime shift, as may have occurred on Dairy Bull Reef in Jamaica (Idjadi et al. 2006). However, the increases in SD were small for some variables, and in one instance, SD de-

creased; examination of local equilibrium dynamics (app. C) revealed the importance of short-term dynamics that may overturn the expected increase in SD arising from critical slowing down (Scheffer et al. 2009). This highlights the point that there is no a priori guarantee that SD for a dynamic variable would increase as a critical threshold is approached, since critical slowing down refers to only long-term dynamics specified by the dominant eigenvalue (Wissel 1984; Neubert and Caswell 1997). Other recent theoretical work has also demonstrated situations, for systems undergoing regime shifts, where SD does not show an increasing trend (Hastings and Wysham 2010; Dakos et al. 2011, 2012).

Furthermore, our results show that detection of an increasing SD trend depends on the window length used for calculation and the rate at which the critical threshold is approached. An overly short window (e.g., 5 years) can miss an increasing SD trend by focusing on only short-term fluctuations, whereas an overly long window (e.g., 100 years) could introduce spurious increases in SD caused by the moving average of each dynamic variable; the latter is evidenced by SD values that are higher than the maximum found for stationary dynamics (fig. 3). This highlights the utility of modeling to identify optimum window lengths that minimize these artifacts by giving increasing SD values that best match values predicted using stationary distributions for the variables considered. In this study,

the optimum length for the SD of coral cover was always much longer than that for the SD of turf algal cover (table 2); furthermore, using the optimum lengths, SD of coral cover typically exhibited longer lags for detection of increased SD predicted by the stationary distributions (table 2). These results reflect the slower coral dynamics and suggest that monitoring turf algal dynamics for early warning signals could require shorter time series from monitoring—often no more than a decade—and be more effective. This is important since empirical time series of coral reef benthic covers typically cover a couple of decades at best (Holmes and Johnstone 2010). Model results also show that as the grazing pressure approached the critical threshold at a greater rate, the optimum lengths typically shortened (table 2), thus aiding detection of an early warning signal. Another encouraging result is that even coarse sampling at once every 3 years typically gave low (<10%) sampling errors in SD trends. This augurs well for detection of early warning signals using data from existing monitoring programs, such as that by the Australian Institute of Marine Science for the Great Barrier Reef (<http://www.aims.gov.au/docs/research/monitoring/reef/reef-monitoring.html>), which samples at an annual rate.

The results for skewness of proportional covers indicated no clear trends except for turf algal cover in the case of decreasing grazing pressure. Even in this case, skewness decreased in contrast to theoretical expectations (as described in “Introduction”; Scheffer et al. 2009). These results are consistent with those of Takimoto (2009), who also found no clear trends for skewness in population abundance for his model of an invading species population with alternative stable states, as a critical threshold in the immigration rate was approached. Guttal and Jayaprakash (2008) did find increasing skewness for two models of a semiarid ecosystem and a model of a lake ecosystem, as critical disturbance thresholds were approached. However, for all three models, stochasticity was introduced using Gaussian noise terms, which, as noted by the authors, could be an oversimplification (Guttal and Jayaprakash 2008).

Overall, our results provide the first theoretical evidence that increasing variances of coral and algal covers over time may be used as warning signals of coral-algal regime shifts in coral reef ecosystems on spatial scales commensurate with observational studies (Hill and Wilkinson 2004; Mumby et al. 2005; García-Salgado et al. 2006; Sandin et al. 2008). They also demonstrate that demographic stochasticity alone can generate warning signals, which supports the case that such signals are intrinsic properties of ecosystems in general.

Detecting and Reversing Regime Shifts beyond the Critical Threshold

An interesting result of this study, which is of particular importance for managers, is that even if the critical parameter threshold has been crossed, it may not be too late to detect, respond to, and ultimately reverse a regime shift (fig. 4). For the model coral reef benthos under study, a warning signal could be detected during a regime shift as a temporary period of stability in coral cover following an initial sharp drop, which should be evident from any long-term monitoring exercise. This period can last for decades, allowing sufficient time to implement management measures to return grazing pressure to a precritical level, hence reversing the regime shift without incurring the costs of hysteresis. The signal may also help management to identify the location of a critical threshold.

Theoretically, the existence of this safety net is predicated on the existence of an unstable saddle point that stalls dynamic convergence to an undesirable stable equilibrium (Strogatz 1994; Hastings 2004). Previous studies have focused on detecting regime shifts before a critical threshold is reached, but some studies have found that convergence to a new stable equilibrium beyond a critical threshold can take a long time, from months to decades (Van Geest et al. 2007; Biggs et al. 2009). Whether the existence of these ghost attractors is common in the dynamics of natural ecosystems is unknown, so a strategy of detecting and reversing a regime shift once it has started should be used only as a last resort.

Spatial Extensions

This study has investigated the effects of demographic stochasticity on the detection of signals that may provide early warning of ecological regime shifts, using a nonspatial coral reef benthic model. A logical extension is to make the model spatially explicit by arranging the discrete benthic units in a spatial pattern of adjacent units. For each benthic unit, probabilities for spatially localized processes, such as overgrowth, would then be a function of the proportional covers of corals, turf algae, and macroalgae derived by considering just neighboring benthic units rather than all units. A spatial model has the advantage of allowing investigation of possible early warning signals calculated from data sampled over space rather than time. Spatial indicators may be particularly useful for ecosystems where available time series are short, such as coral reefs (Holmes and Johnstone 2010). Previous studies have developed and used spatial models of arid ecosystems undergoing desertification (Dakos et al. 2011), lakes exposed to eutrophication (Dakos et al. 2010; Donangelo et al. 2010), and vegetation experiencing increased grazing

(Guttal and Jayaprakash 2009; Dakos et al. 2010) to test candidate spatial indicators. These studies have provided evidence of increasing spatial variance (Guttal and Jayaprakash 2009; Donangelo et al. 2010; Dakos et al. 2011), skewness (Guttal and Jayaprakash 2009; Dakos et al. 2011), and correlation (Dakos et al. 2010, 2011) before a critical disturbance threshold. Characteristic spatial patterns reflecting self-organized patchiness have also been found preceding a critical threshold (Rietkerk et al. 2002, 2004; Donangelo et al. 2010; Dakos et al. 2011).

However, to date there have been no studies of early warning signals using a spatial coral reef model, especially one that models demographic stochasticity in the way presented in this study. Of interest is the set of spatial signals that can be identified in such a model preceding a discontinuous coral-algal regime shift. Donangelo et al. (2010) found for their spatial lake model that spatial variance increased earlier than temporal variance as a critical average nutrient input rate was approached. A similar comparison between spatial and temporal signals can usefully be performed for a spatial coral reef model to quantify the relative utility of the two indicator types in a management context. As a first step toward this kind of analysis, we have developed a spatial version of the stochastic model used in this study with 1,000 discrete benthic units arranged in a 25×40 grid (for details, see app. E). Importantly, preliminary results demonstrate that as grazing pressure decreases to a critical threshold, this spatial model replicates the trends in (temporal) SD and skewness found in this study (app. E), showing that these trends are robust to the addition of spatial structure.

Other Future Perspectives

Apart from spatial extensions, another logical extension to this study is to add environmental stochasticity to demographic stochasticity and investigate their combined effects on signal detection. This could be done using either the coral reef model in this study or another model for which the stochastic framework presented here could be applied. The framework can readily be adapted to also include environmental stochasticity by allowing one or more model parameters to vary randomly in each time step, according to defined probability distributions. In addition, one or more of the model variables can be perturbed by noise terms defined by probability distributions. By modeling different degrees of demographic and environmental stochasticity, the relative importance of each to the detection of warning signals could be established. A potential obstacle here is that the variance of population parameters due to environmental stochasticity could be poorly known for most populations (Engen et al. 1998).

Finally, there remains the different but related issue of

quantitatively determining how close a system is to a critical parameter threshold, which cannot be deduced from trends in SD alone. Thus, results from modeling studies of trends in early warning signals, such as this study, should be complemented with those focused on estimating threshold values of a parameter (e.g., Marzloff et al. 2013). The former type of study would identify statistics for system variables expected to give a trend as a parameter threshold is reached; if monitoring of these statistics in a real system yields the predicted trends, then this provides evidence to managers that the system (1) is capable of sudden, non-linear regime shifts, which is not guaranteed to be the case (Scheffer et al. 2001; Fung et al. 2011; Marzloff et al. 2011), and (2) is moving toward such a regime shift because of changing values of the parameter considered. The latter type of study would give estimates of critical threshold values of the parameter considered, ideally with uncertainty bounds; monitoring of the parameter in the managed system would then allow quantification of how far the system is likely to be from the critical threshold. Alternatively, instead of estimating threshold values of a parameter, threshold values for the statistics could be estimated. This is advantageous for management if values of the parameter cannot be estimated because of logistical reasons, such as cost or technological constraints. Yet another option would be to estimate threshold values for both the parameter and the statistics, if both can be monitored. This would allow a more precautionary approach where the system is managed such that neither the threshold for the parameter nor the thresholds for the statistics are exceeded.

Acknowledgments

We would like to thank two anonymous reviewers whose comments and suggestions have led to substantial improvements in the manuscript. In addition, we thank all members of the Modeling and Decision Support Working Group of the Coral Reef Targeted Research and Capacity Building for Management Project (CRTR-CBMP) for insightful discussion and generous support throughout this project. T.F. was supported by a grant from the Engineering and Physical Sciences Research Council and is now supported by a Beaufort Marine Research Award, carried out under the "Sea Change" Strategy and the Strategy for Science Technology and Innovation (2006–2013), with the support of the Marine Institute, funded under the Marine Research Sub-Programme of the Irish National Development Plan 2007–2013. Furthermore, all authors were supported by funding from the CRTR-CBMP.

Literature Cited

- Akçakaya, H. R. 1991. A method for simulating demographic stochasticity. *Ecological Modelling* 54:133–136.
- Beisner, B. E., D. T. Haydon, and K. Cuddington. 2003. Alternative stable states in ecology. *Frontiers in Ecology and the Environment* 1:376–382.
- Biggs, R., S. R. Carpenter, and W. A. Brock. 2009. Turning back from the brink: detecting an impending regime shift in time to avert it. *Proceedings of the National Academy of Sciences of the USA* 106:826–831.
- Bjørnstad, O. N., and B. T. Grenfell. 2001. Noisy clockwork: time series analysis of population fluctuations in animals. *Science* 298:638–643.
- Brock, W. A., and S. R. Carpenter. 2006. Variance as a leading indicator of regime shift in ecosystem services. *Ecology and Society* 11:9. <http://www.ecologyandsociety.org/vol11/iss2/art9/>.
- . 2010. Interacting regime shifts in ecosystems: implication for early warnings. *Ecological Monographs* 80:353–367.
- Carpenter, S. R., and W. A. Brock. 2006. Rising variance: a leading indicator of ecological transition. *Ecology Letters* 9:311–318.
- . 2011. Early warnings of unknown nonlinear shifts: a non-parametric approach. *Ecology* 92:2196–2201.
- Carpenter, S. R., W. A. Brock, J. J. Cole, J. F. Kitchell, and M. L. Pace. 2008. Leading indicators of trophic cascades. *Ecology Letters* 11:128–138.
- Carpenter, S. R., J. J. Cole, M. L. Pace, R. Batt, W. A. Brock, T. Cline, J. Coloso, et al. 2011. Early warnings of regime shifts: a whole-ecosystem experiment. *Science* 332:1079–1082.
- Caswell, H. 2001. *Matrix population models: construction, analysis, and interpretation*. 2nd ed. Sinauer, Sunderland, MA.
- Chisholm, R. A., and E. Filotas. 2009. Critical slowing down as an indicator of transitions in two-species models. *Journal of Theoretical Biology* 257:142–149.
- Contamin, R., and A. M. Ellison. 2009. Indicators of regime shifts in ecological systems: what do we need to know and when do we need to know it? *Ecological Applications* 19:799–816.
- Dai, L., D. Vorselen, K. S. Korolev, and J. Gore. 2012. Generic indicators for loss of resilience before a tipping point leading to population collapse. *Science* 336:1175–1177.
- Dakos, V., S. Kéfi, M. Rietkerk, E. H. van Nes, and M. Scheffer. 2011. Slowing down in spatially patterned ecosystems at the brink of collapse. *American Naturalist* 177:E153–E166.
- Dakos, V., M. Scheffer, E. H. van Nes, V. Brovkin, V. Petoukhov, and H. Held. 2008. Slowing down as an early warning signal for abrupt climate change. *Proceedings of the National Academy of Sciences of the USA* 105:14308–14312.
- Dakos, V., E. H. van Nes, P. D'Odorico, and M. Scheffer. 2012. Robustness of variance and autocorrelation as indicators of critical slowing down. *Ecology* 93:264–271.
- Dakos, V., E. H. van Nes, R. Donangelo, H. Fort, and M. Scheffer. 2010. Spatial correlation as leading indicator of catastrophic shifts. *Theoretical Ecology* 3:163–174.
- Dayton, P. K. 1971. Competition, disturbance, and community organization: the provision and subsequent utilization of space in a rocky intertidal community. *Ecological Monographs* 41:351–389.
- Donangelo, R., H. Fort, V. Dakos, M. Scheffer, and E. H. van Nes. 2010. Early warnings for catastrophic shifts in ecosystems: comparison between spatial and temporal indicators. *International Journal of Bifurcation and Chaos* 20:315–321.
- Drake, J. M., and B. D. Griffen. 2010. Early warning signals of extinction in deteriorating environments. *Nature* 467:456–459.
- Engen, S., Ø. Bakke, and A. Islam. 1998. Demographic and environmental stochasticity: concepts and definitions. *Biometrics* 54:840–846.
- Folke, C., S. Carpenter, B. Walker, M. Scheffer, T. Elmqvist, L. Gunderson, and C. S. Holling. 2004. Regime shifts, resilience, and biodiversity in ecosystem management. *Annual Review of Ecology, Evolution, and Systematics* 35:557–581.
- Fung, T., R. M. Seymour, and C. R. Johnson. 2011. Alternative stable states and phase shifts in coral reefs under anthropogenic stress. *Ecology* 92:967–982.
- García-Salgado, M., T. Camarena-Luhurs, G. Gold, M. Vasquez, G. Galland, G. Nava, G. Alarcón, and V. Ceja. 2006. *Baseline of the status of the Mesoamerican Barrier Reef Systems*. Belize City.
- Gilpin, M. 1992. Demographic stochasticity: a Markovian approach. *Journal of Theoretical Biology* 154:1–8.
- Guckenheimer, J., and P. Holmes. 1997. *Nonlinear oscillations, dynamical systems, and bifurcations of vector fields*. Springer, New York.
- Guttal, V., and C. Jayaprakash. 2008. Changing skewness: an early warning signal of regime shifts in ecosystems. *Ecology Letters* 11:450–460.
- . 2009. Spatial variance and spatial skewness: leading indicators of regime shifts in spatial ecological systems. *Theoretical Ecology* 2:3–12.
- Hartl, D. L., and A. G. Clark. 1997. *Principles of population genetics*. 3rd ed. Sinauer, Sunderland, MA.
- Hastings, A. 2004. Transients: the key to long-term ecological understanding? *Trends in Ecology and Evolution* 19:39–45.
- . 2010. Timescales, dynamics, and ecological understanding. *Ecology* 91:3471–3480.
- Hastings, A., and D. B. Wysham. 2010. Regime shifts in ecological systems can occur with no warning. *Ecology Letters* 13:464–472.
- Hill, J., and C. Wilkinson. 2004. *Methods for ecological monitoring of coral reefs*. Version 1. Australian Institute of Marine Science, Townsville.
- Hirota, M., M. Holmgren, E. H. van Nes, and M. Scheffer. 2011. Global resilience of tropical forest and savannah to critical transitions. *Science* 334:232–235.
- Holling, C. S. 1973. Resilience and stability of ecological systems. *Annual Review of Ecology, Evolution, and Systematics* 4:1–23.
- Holmes, G., and R. W. Johnstone. 2010. Modelling coral reef ecosystems with limited observational data. *Ecological Modelling* 221:1173–1183.
- Hughes, T. P. 1994. Catastrophes, phase shifts, and large-scale degradation of a Caribbean coral reef. *Science* 265:1547–1551.
- Idjadi, J. A., S. C. Lee, J. F. Bruno, W. F. Precht, L. Allen-Requa, and P. J. Edmunds. 2006. Rapid phase-shift reversal on a Jamaican coral reef. *Coral Reefs* 25:209–211.
- Kelsey, J., B. Henderson, R. Seymour, and A. Hone. 2008. A stochastic model of the Interleukin (IL)-1 β network. Pages 1–11 in P. J. Bentley, D. Lee, and S. Jung, eds. *Proceedings of the 7th International Conference on Artificial Immune Systems (ICARIS 2008)*, LNCS Volume 5132. Springer, Berlin.
- Kinlan, B. P., S. D. Gaines, and S. E. Lester. 2005. Propagule dispersal and the scales of marine community process. *Diversity and Distributions* 11:139–148.
- Kleinen, T., H. Held, and G. Petschel-Held. 2003. The potential role of spectral properties in detecting thresholds in the Earth system:

- application to the thermohaline circulation. *Ocean Dynamics* 53: 53–63.
- Knowlton, N. 1992. Threshold and multiple stable states in coral reef community dynamics. *American Zoologist* 32:674–682.
- Konar, B., and J. A. Estes. 2003. The stability of boundary regions between kelp beds and deforested areas. *Ecology* 84:174–185.
- Lande, R. 1993. Risks of population extinction from demographic and environmental stochasticity and random catastrophes. *American Naturalist* 142:911–927.
- Lessios, H. A. 1988. Mass mortality of *Diadema antillarum* in the Caribbean: what have we learned. *Annual Review of Ecology, Evolution, and Systematics* 19:371–393.
- Ling, S. D., C. R. Johnson, S. D. Frusher, and K. R. Ridgway. 2009. Overfishing reduces resilience of kelp beds to climate-driven catastrophic phase shift. *Proceedings of the National Academy of Sciences of the USA* 106:22341–22345.
- MacArthur, R., and R. Levins. 1967. The limiting similarity, convergence, and divergence of coexisting species. *American Naturalist* 101:377–385.
- Marzloff, M. P., J. M. Dambacher, C. R. Johnson, L. R. Little, and S. D. Frusher. 2011. Exploring alternative states in ecological systems with a qualitative analysis of community feedback. *Ecological Modelling* 222:2651–2662.
- Marzloff, M. P., C. R. Johnson, L. R. Little, J.-C. Soulié, and S. D. Ling. 2013. Sensitivity analysis and pattern-oriented validation of TRITON, a model with alternative community states: insights on temperate rocky reefs dynamics. *Ecological Modelling* 258:16–32.
- May, R. M. 1977. Thresholds and breakpoints in ecosystems with a multiplicity of stable states. *Nature* 269:471–477.
- Maynard Smith, J., and J. Haigh. 1974. The hitch-hiking effect of a favourable gene. *Genetics Research* 23:23–35.
- Mikosch, T. 1998. *Elementary stochastic calculus with finance in view*. World Scientific, Singapore.
- Mumby, P. J., N. L. Foster, and E. A. G. Fahy. 2005. Patch dynamics of coral reef macroalgae under chronic and acute disturbance. *Coral Reefs* 24:681–692.
- Mumby, P. J., A. Hastings, and H. J. Edwards. 2007. Thresholds and the resilience of Caribbean coral reefs. *Nature* 450:98–101.
- Nakajima, H., and D. L. DeAngelis. 1989. Resilience and local stability in a nutrient-limited resource-consumer system. *Bulletin of Mathematical Biology* 51:501–510.
- Neubert, M. G., and H. Caswell. 1997. Alternatives to resilience for measuring the responses of ecological systems to perturbations. *Ecology* 78:653–665.
- Øksendal, B. 1995. *Stochastic differential equations*. Springer, New York.
- Petraitis, P. S., and S. R. Dudgeon. 2004. Detection of alternative stable states in marine communities. *Journal of Experimental Marine Biology and Ecology* 300:343–371.
- Rietkerk, M., M. C. Boerlijst, F. van Langevelde, R. HilleRisLambers, J. van de Koppel, L. Kumar, H. H. T. Prins, et al. 2002. Self-organization of vegetation in arid ecosystems. *American Naturalist* 160:524–530.
- Rietkerk, M., S. C. Dekker, P. C. de Ruiter, and J. van de Koppel. 2004. Self-organized patchiness and catastrophic shifts in ecosystems. *Science* 305:1926–1929.
- Sandin, S. A., J. E. Smith, E. E. DeMartini, E. A. Dinsdale, S. D. Donner, A. M. Friedlander, T. Konotchick, et al. 2008. Baselines and degradation of coral reefs in the Northern Line Islands. *PLoS ONE* 3:e1548.
- Schaffer, M. L. 1981. Minimum population sizes for species conservation. *BioScience* 31:131–134.
- . 1983. Determining minimum viable population sizes for the grizzly bear. *International Conference on Bear Research and Management* 5:133–139.
- Scheffer, M., J. Bascompte, W. A. Brock, V. Brovkin, S. R. Carpenter, V. Dakos, H. Held, et al. 2009. Early-warning signals for critical transitions. *Nature* 461:53–59.
- Scheffer, M., and S. R. Carpenter. 2003. Catastrophic regime shifts in ecosystems: linking theory to observation. *Trends in Ecology and Evolution* 18:648–656.
- Scheffer, M., S. Carpenter, J. A. Foley, C. Folke, and B. Walker. 2001. Catastrophic shifts in ecosystems. *Nature* 413:591–596.
- Schröder, A., L. Persson, and A. M. De Roos. 2005. Direct experimental evidence for alternative stable states: a review. *Oikos* 110: 3–19.
- Spencer, M., and J. E. Tanner. 2008. Lotka-Volterra competition models for sessile organisms. *Ecology* 89:1134–1143.
- Strogatz, S. H. 1994. *Nonlinear dynamics and chaos, with applications to physics, biology, chemistry, and engineering*. Perseus, New York.
- Szmant, A. M. 2002. Nutrient enrichment on coral reefs: is it a major cause of coral reef decline? *Estuaries* 25:743–766.
- Takimoto, G. 2009. Early warning signals of demographic regime shifts in invading populations. *Population Ecology* 51:419–426.
- Van Geest, G. J., H. Coops, M. Scheffer, and E. H. van Nes. 2007. Long transients near the ghost of a stable state in eutrophic shallow lakes with fluctuating water levels. *Ecosystems* 10:36–46.
- van Nes, E. H., and M. Scheffer. 2003. Alternative attractors may boost uncertainty and sensitivity in ecological models. *Ecological Modelling* 159:117–124.
- . 2007. Slow recovery from perturbations as a generic indicator of a nearby catastrophic shift. *American Naturalist* 169:738–747.
- Veraart, A. J., E. J. Faassen, V. Dakos, E. H. van Nes, M. Lürling, and M. Scheffer. 2012. Recovery rates reflect distance to a tipping point in a living system. *Nature* 481:357–359.
- Wissel, C. 1984. A universal law of the characteristic return time near thresholds. *Oecologia (Berlin)* 65:101–107.

Associate Editor: Daniel L. Roelke
Editor: Troy Day

Appendix A from T. Fung et al., “Warning Signals of Regime Shifts as Intrinsic Properties of Endogenous Dynamics”

(Am. Nat., vol. 182, no. 2, p. 208)

Framework for Adding Demographic Stochasticity to Deterministic Dynamics: Application to a Coral Reef Benthic Model

Demographic stochasticity is introduced into the deterministic coral reef benthic model specified by equations (1)–(3) (Fung et al. 2011), using a framework that utilizes a Markov process. This framework involves splitting the benthic area modeled into discrete units of equal size and then defining transition probabilities for the state that each unit can take over the course of a discrete time step. Let the number of discrete benthic units be N . There are four states, indexed by $\mathbf{S} = \{0, 1, 2, 3\}$. Let the corresponding system state vector be $\mathbf{N} = \{N_0, N_1, N_2, N_3\}$, where N_0 , N_1 , N_2 , and N_3 are the number of units occupied by corals, turf algae, macroalgae, and space, respectively. Hence, the proportional covers of corals, turf algae, macroalgae, and space are defined by $C = N_0/N$, $T = N_1/N$, $M = N_2/N$, and $S = N_3/N$, respectively. Let the proportional cover state vector be $\mathbf{s} = \{s_0, s_1, s_2, s_3\} = \{C, T, M, S\}$. During each discrete time step, each unit either remains in the same state or moves into another state. The probability of a unit in state i being in state j in the next time step, p_{ij} , is defined as a function of the probabilities of elementary events; these are events that cause a change $\mathbf{N} \rightarrow \mathbf{N} + \mathbf{E}$, where the system state change vector $\mathbf{E} = (\varepsilon_0, \varepsilon_1, \varepsilon_2, \varepsilon_3)$ satisfies $\varepsilon_u \in \{0, \pm 1\}$ and $\sum_u \varepsilon_u = 1$ for $u \in \mathbf{S}$. The corresponding change in the proportional cover state vector is $\mathbf{s} \rightarrow \mathbf{s} + \Delta\mathbf{s}\mathbf{E}$, where $\Delta s = 1/N$. Let the set of all possible system state change vectors be

$$\mathbf{Z} \subset \left\{ \mathbf{E} = (\varepsilon_0, \varepsilon_1, \varepsilon_2, \varepsilon_3); \varepsilon_u \in \{0, \pm 1\}, \sum_{u=0}^3 \varepsilon_u = 1 \right\}. \quad (\text{A1})$$

Let E be the set of all possible elementary events. E is partitioned into the form

$$E = \bigsqcup_{u=0}^3 E_u, \quad (\text{A2})$$

a disjoint union. Thus, each event is associated with a system unit in state u . In addition, each set E_u has a distinguished elementary event \emptyset representing “nothing happens.” A system unit in state u is only susceptible to events in E_u .

For each elementary event $e \in E$, there is a conditional probability $p(e|\mathbf{s})$ per system unit in state u , which satisfies

$$\sum_{e \in E_u} p(e|\mathbf{s}) = 1. \quad (\text{A3})$$

In one discrete time step, a single elementary event occurs simultaneously to each of the N system units. The term “simultaneous” here is taken to mean that all events occur under the same conditions; that is, the system state \mathbf{s} remains the same for all events. Only at the end of the time step is the system state updated. If the N elementary events produce changes of (system) state $\mathbf{E}_1, \dots, \mathbf{E}_N$, then the state change at the updating time is $\mathbf{E}^{(N)} = \mathbf{E}_1 + \dots + \mathbf{E}_N$. We shall show that these changes of state, occurring in discrete time steps, define a Markov process on Ω_N , which is the rational lattice defined by

$$\Omega_N = \{ \mathbf{s} \in \Delta[\mathbf{S}]; Ns_u = N_u \text{ is an integer for each } u \in \mathbf{S} \}, \quad (\text{A4})$$

where $\Delta[\mathbf{S}]$ is the four-dimensional simplex over the set of states \mathbf{S} , given by

$$\Delta[\mathbf{S}] = \left\{ \mathbf{s} = (s_0, s_1, s_2, s_3) \in \mathbf{R}^4; 0 \leq s_u \leq 1, \sum_{u=0}^3 s_u = 1 \right\}. \quad (\text{A5})$$

To define a Markov process, we must define transition probabilities $p(\mathbf{s}'|\mathbf{s})$ for all possible (proportional cover) state changes $\mathbf{s} \rightarrow \mathbf{s}'$ ($\mathbf{s}, \mathbf{s}' \in \Omega_N$) and satisfying

$$\sum_{\mathbf{s}' \in \Omega_N} p(\mathbf{s}'|\mathbf{s}) = 1 \quad (\text{A6})$$

for each $\mathbf{s} \in \Omega_N$. Let the N system units be indexed so that units in the same state occur consecutively. Thus, set $K_{-1} = 0$ and $K_u = K_{u-1} + N_u$ for $0 \leq u \leq 3$ and define

$$E^N(\mathbf{s}) = E_0^{N_0} \times E_1^{N_1} \times E_2^{N_2} \times E_3^{N_3} = \{(e_1, \dots, e_N) \in E^N: e_{K_{u-1}+i} \in E_u, 1 \leq i \leq N_u, u \in \mathbf{S}\}. \quad (\text{A7})$$

In addition, define

$$E^N(\mathbf{E}^{(N)}|\mathbf{s}) = \left\{ \mathbf{e} \in E^N(\mathbf{s}): \sum_{i=1}^N \mathbf{E}(e_i) = \mathbf{E}^{(N)} \right\}, \quad (\text{A8})$$

where $\mathbf{E}(e)$ is the system state change due to the elementary event e . Then define transition probabilities $p(\mathbf{s}'|\mathbf{s})$ by $p(\mathbf{s}'|\mathbf{s}) = 0$ unless $\mathbf{s}' = \mathbf{s} + \Delta\mathbf{s}\mathbf{E}^{(N)}$ and

$$p(\mathbf{s} + \Delta\mathbf{s}\mathbf{E}^{(N)}|\mathbf{s}) = \sum_{\mathbf{e} \in E^N(\mathbf{E}^{(N)}|\mathbf{s})} \prod_{i=1}^N p(e_i|\mathbf{s}). \quad (\text{A9})$$

To check that these define transition probabilities for a Markov process, we have:

$$\begin{aligned} \sum_{\mathbf{s}'} p(\mathbf{s}'|\mathbf{s}) &= \sum_{\mathbf{E}^{(N)}} p(\mathbf{s} + \Delta\mathbf{s}\mathbf{E}^{(N)}|\mathbf{s}) \\ &= \sum_{\mathbf{e} \in E^N(\mathbf{s})} \prod_{i=1}^N p(e_i|\mathbf{s}) \\ &= \prod_{u \in \mathbf{S}} \left(\sum_{\mathbf{e}_u \in E_u^{N_u}} \prod_{i=1}^{N_u} p(e_{u,i}|\mathbf{s}) \right) \text{ (using eq. [A7] to write } \mathbf{e} = \mathbf{e}_0 \times \mathbf{e}_1 \times \mathbf{e}_2 \times \mathbf{e}_3, \text{ with } \mathbf{e}_u \in E_u^{N_u}\text{)} \\ &= \prod_{u \in \mathbf{S}} \left(\sum_{e \in E_u} p(e|\mathbf{s}) \right)^{N_u} \\ &= \prod_{u \in \mathbf{S}} (1)^{N_u} \\ &= 1, \end{aligned}$$

as required.

For the CTMm, the elementary events are as follows:

- $e1$. Mortality of coral, with state change vector $\mathbf{E} = (-1, 0, 0, 1)$ and probability (per unit of existing coral) of $p(e1|\mathbf{s}) = d_c \delta t$.
- $e2$. Growth of macroalgae over coral, with state change vector $\mathbf{E} = (-1, 0, 1, 0)$ and probability (per unit of existing coral) of $p(e2|\mathbf{s}) = \gamma_{CM} r_M M \delta t$.
- $e3$. Recruitment of spawning coral onto turf algae, with state change vector $\mathbf{E} = (1, -1, 0, 0)$ and probability (per unit of existing turf algae) of $p(e3|\mathbf{s}) = \varepsilon_c l_c^s \delta t$.
- $e4$. Recruitment of brooding coral onto turf algae, with state change vector $\mathbf{E} = (1, -1, 0, 0)$ and probability (per unit of existing turf algae) of $p(e4|\mathbf{s}) = \varepsilon_c l_c^b C \delta t$.
- $e5$. Growth of coral over turf algae, with state change vector $\mathbf{E} = (1, -1, 0, 0)$ and probability (per unit of existing turf algae) of $p(e5|\mathbf{s}) = \alpha_c r_c (1 - \beta_M M) C \delta t$.
- $e6$. Grazing on turf algae, with state change vector $\mathbf{E} = (0, -1, 0, 1)$ and probability (per unit of existing turf algae) of $p(e6|\mathbf{s}) = g_T \theta \delta t$.
- $e7$. Growth of macroalgae over turf algae, with state change vector $\mathbf{E} = (0, -1, 1, 0)$ and probability (per unit of existing turf algae) of $p(e7|\mathbf{s}) = \gamma_{TM} r_M M \delta t$.
- $e8$. Grazing on macroalgae, with state change vector $\mathbf{E} = (0, 0, -1, 1)$ and probability (per unit of existing macroalgae) of $p(e8|\mathbf{s}) = g_M \theta \delta t$.
- $e9$. Recruitment of spawning coral onto space, with state change vector $\mathbf{E} = (1, 0, 0, -1)$ and probability (per unit of existing space) of $p(e9|\mathbf{s}) = l_c^s \delta t$.

- e*10. Recruitment of brooding coral onto space, with state change vector $\mathbf{E} = (1, 0, 0, -1)$ and probability (per unit of existing space) of $p(e10|\mathbf{s}) = l_c^b C \delta t$.
- e*11. Growth of coral over space, with state change vector $\mathbf{E} = (1, 0, 0, -1)$ and probability (per unit of existing space) of $p(e11|\mathbf{s}) = r_c(1 - \beta_M M) C \delta t$.
- e*12. Growth of turf algae from space, with state change vector $\mathbf{E} = (0, 1, 0, -1)$ and probability (per unit of existing space) of $p(e12|\mathbf{s}) = \zeta_T(1 - \theta) \delta t$.
- e*13. Growth of macroalgae onto space, with state change vector $\mathbf{E} = (0, 0, 1, -1)$ and probability (per unit of existing space) of $p(e13|\mathbf{s}) = r_M M \delta t$.

Thus,

$$E_0 = \{\emptyset, e1, e2\}, \quad (\text{A10a})$$

$$E_1 = \{\emptyset_1, e3, e4, e5, e6, e7\}, \quad (\text{A10b})$$

$$E_2 = \{\emptyset_2, e8\}, \quad (\text{A10c})$$

$$E_3 = \{\emptyset_3, e9, e10, e11, e12, e13\}. \quad (\text{A10d})$$

It is required that $f_u(\mathbf{s}) = p(E_u/\emptyset_u) \leq 1$ for $u \in \mathbf{S}$. For the time step used in this study, which is $\delta t = 1$ day, and the parameter ranges derived by Fung et al. (2011), this is always true. The probabilities in the transition matrix, p_{ij} , can then be calculated by summation of probabilities of elementary events in E_i that result in a transition to state j . This gives the transition matrix shown in equation (4), where the symbols in the matrix are given by

$$g_{CM} = p(e2|\mathbf{s}) = \gamma_{CM} r_M M \delta t, \quad (\text{A11a})$$

$$g_{TC} = p(e5|\mathbf{s}) = \alpha_C r_C (1 - \beta_M M) C \delta t, \quad (\text{A11b})$$

$$g_{TM} = p(e7|\mathbf{s}) = \gamma_{TM} r_M M \delta t, \quad (\text{A11c})$$

$$g_{SC} = p(e11|\mathbf{s}) = r_c(1 - \beta_M M) C \delta t, \quad (\text{A11d})$$

$$g_{ST} = p(e12|\mathbf{s}) = \zeta_T(1 - \theta) \delta t, \quad (\text{A11e})$$

$$g_{SM} = p(e13|\mathbf{s}) = r_M M \delta t, \quad (\text{A11f})$$

$$m_{CS} = p(e1|\mathbf{s}) = d_C \delta t, \quad (\text{A11g})$$

$$m_{TS} = p(e6|\mathbf{s}) = g_T \theta \delta t, \quad (\text{A11h})$$

$$m_{MS} = p(e8|\mathbf{s}) = g_M \theta \delta t, \quad (\text{A11i})$$

$$r_{TC} = p(e3|\mathbf{s}) + p(e4|\mathbf{s}) = (\varepsilon_C l_C^s + \varepsilon_C l_C^b C) \delta t, \quad (\text{A11j})$$

$$r_{SC} = p(e9|\mathbf{s}) + p(e10|\mathbf{s}) = (l_C^s + l_C^b C) \delta t. \quad (\text{A11k})$$

Equations (A11) give rise to equations (5).

Mean Field (Expected) Dynamics

The system state vector is $\mathbf{N} = \{N_0, N_1, N_2, N_3\}$, and at each updating time step, $\mathbf{E}_1, \dots, \mathbf{E}_N$ are the state change vectors associated with the system units. As above, let $K_{-1} = 0$ and $K_u = N_0 + \dots + N_u$. Then the N_u system units with state u have associated state changes labeled $\mathbf{E}_{K_{u-1}+1}, \dots, \mathbf{E}_{K_u}$. The probability that the i th system unit in state u undergoes state change $\mathbf{E}_{K_{u-1}+i}$ is

$$\sum_{e \in E_u(\mathbf{E}_{K_{u-1}+i})} p(e|\mathbf{s}), \quad (\text{A12})$$

from which it follows that the corresponding expected change in \mathbf{s} is

$$\Delta s \sum_{\mathbf{E}_{K_{u-1}+i} \in \mathbf{Z}} \mathbf{E}_{K_{u-1}+i} \sum_{e \in E_u(\mathbf{E}_{K_{u-1}+i})} p(e|\mathbf{s}) = \Delta s \sum_{\mathbf{E} \in \mathbf{Z}} \mathbf{E} \sum_{e \in E_u(\mathbf{E})} p(e|\mathbf{s}). \quad (\text{A13})$$

This is the same for each system unit in state u . Hence, the expected change in \mathbf{s} due to all of the N_u system units in

state u is

$$\begin{aligned}
 \Delta s & \sum_{i=1}^{N_u} \sum_{\mathbf{E} \in \mathbf{Z}} \mathbf{E} \sum_{e \in E_u(\mathbf{E})} p(e|\mathbf{s}) \\
 & = \Delta s N_u \sum_{\mathbf{E} \in \mathbf{Z}} \mathbf{E} \sum_{e \in E_u(\mathbf{E})} p(e|\mathbf{s}) \\
 & = \sum_{\mathbf{E} \in \mathbf{Z}} \mathbf{E} \sum_{e \in E_u(\mathbf{E})} p(e|\mathbf{s}) s_u.
 \end{aligned} \tag{A14}$$

Finally, the expected change in \mathbf{s} due to all the system units is

$$\begin{aligned}
 \exp[\Delta \mathbf{s}|\mathbf{s}] & = \sum_{u \in \mathbf{S}} \sum_{\mathbf{E} \in \mathbf{Z}} \mathbf{E} \sum_{e \in E_u(\mathbf{E})} p(e|\mathbf{s}) s_u \\
 & = \sum_{\mathbf{E} \in \mathbf{Z}} \mathbf{E} \sum_{u \in \mathbf{S}} \sum_{e \in E_u(\mathbf{E})} p(e|\mathbf{s}) s_u \\
 & = \sum_{\mathbf{E} \in \mathbf{Z}} \mathbf{E} p(\mathbf{s} + \Delta s \mathbf{E}|\mathbf{s}) \\
 & = \bar{\mathbf{E}}(\mathbf{s}).
 \end{aligned} \tag{A15}$$

Thus, the mean field dynamics associated with simultaneous updating is

$$\mathbf{s}' = \mathbf{s} + \bar{\mathbf{E}}(\mathbf{s}), \tag{A16}$$

which is exactly the same as the numerical approximation of the set of differential equations (1)–(3) using Euler's method. Therefore, with a small time step of 1 day, the mean field dynamics are a close approximation of the deterministic dynamics given by the differential equations. In fact, with a time step of 1 day, Euler's method gives dynamics for the set of differential equations that are very close to that obtained using fourth-order Runge-Kutta. One thousand simulations with 1,000 randomly chosen parameter sets (using parameter ranges from Fung et al. 2011) and initial conditions, each lasting 500 years, show that the maximum difference using the two methods is <0.0003 for any of the four proportional covers and at any time step.

Literature Cited in Appendix A

Fung, T., R. M. Seymour, and C. R. Johnson. 2011. Alternative stable states and phase shifts in coral reefs under anthropogenic stress. *Ecology* 92:967–982.

Appendix B from T. Fung et al., “Warning Signals of Regime Shifts as Intrinsic Properties of Endogenous Dynamics”

(Am. Nat., vol. 182, no. 2, p. 208)

Parameter Sets Used and Example Stationary Dynamics

The set of parameters used to draw the phase diagram in figure 1A is given in table B1. This is the same set of parameters as that used by Fung et al. (2011) to draw their figure 3C. The set of parameters used to draw the phase diagram in figure 1B is also given in table B1. In addition, the set of parameters used for the simulation in figure D3, which shows a phase shift reversal for the case of nutrient enrichment, is shown in table B1.

For 1,000 discrete benthic units and the parameter set used to draw the phase diagram in figure 1A, figure B1 shows time dynamics for $\theta = 0.85$ and 0.35 , with initial proportional covers allowing convergence to the stationary state with high mean coral cover. These two cases represent dynamics far away from and close to the critical threshold of 0.312 , respectively; closer to the threshold, stationary dynamics show greater variance, most pronounced for turf algal proportional cover. In both cases, stationarity is reached after 500 years.

Table B1. Parameter sets used to draw the phase diagrams in figure 1 together with the parameter set used for figure D3 in appendix D

Parameter	Figure 1A	Figure 1B	Figure D3
θ	.1-.9	.1-.9	.6
d_C (year ⁻¹)	.05	.05	.05
l_C^b (year ⁻¹)	.0009	.0009	.0009
l_C^s (year ⁻¹)	.00006	.00006	.00006
r_C (year ⁻¹)	.2	.2	.2
α_C	.25	.25	.2
ϵ_C	.1	.1	.05
g_T (year ⁻¹)	10	10	9
ζ_T (year ⁻¹)	5	5	11-19.5
g_M (year ⁻¹)	.5	.5	.5
r_M (year ⁻¹)	.35	.7	.35-.62
β_M	.9	.9	.9
γ_{CM}	.1	.1	.1
γ_{TM}	.9	.9	.9

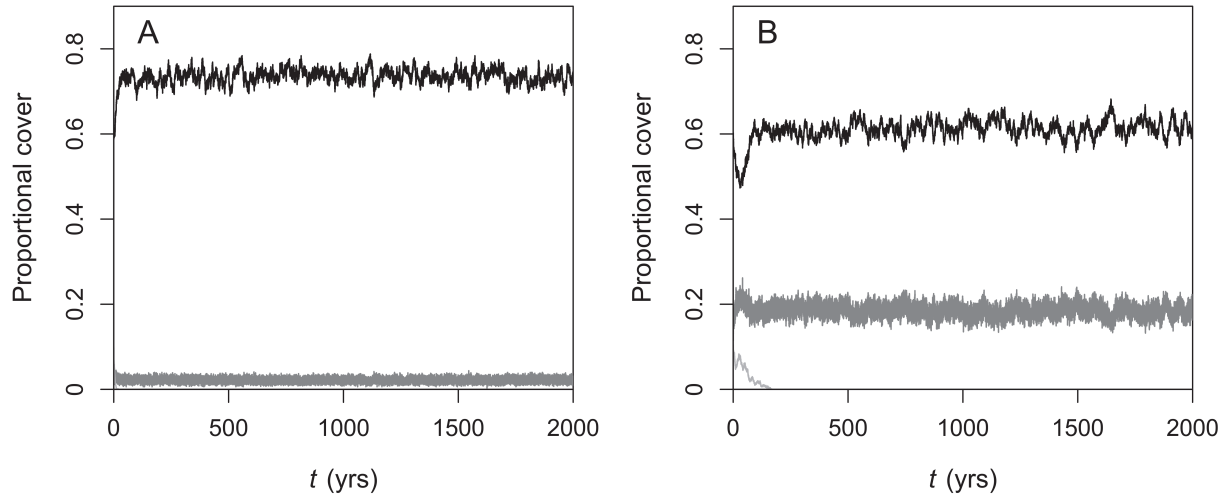


Figure B1: Stochastic coral reef benthic model runs with the parameter set used to draw the phase diagram in figure 1A, with grazing pressure parameter θ set to two different values. Black, dark gray, and light gray lines are the proportional covers of corals, turf algae, and macroalgae, respectively. One thousand discrete benthic units were used, and dynamics were simulated for 2,000 years. In both cases, the initial proportional covers of corals, turf algae, and macroalgae are 0.6, 0.1, and 0.1, respectively. A, $\theta = 0.85$, far away from the critical value of 0.312. Macroalgal cover decreases to 0 quickly, within 21 years. B, $\theta = 0.35$, close to the critical value of 0.312.

Literature Cited in Appendix B

Fung, T., R. M. Seymour, and C. R. Johnson. 2011. Alternative stable states and phase shifts in coral reefs under anthropogenic stress. *Ecology* 92:967–982.

Appendix C from T. Fung et al., “Warning Signals of Regime Shifts as Intrinsic Properties of Endogenous Dynamics” (Am. Nat., vol. 182, no. 2, p. 208)

Mathematical Analysis Showing How the Standard Deviation of Turf Algal Cover Could Decrease Approaching a Critical Threshold

For the set of parameters used to draw the phase diagram in figure 1B, trends in SD as $\theta \rightarrow \theta_c^+ = 0.839$ from 0.1 are shown in figure C1A. SD for T exhibited an increasing trend up to $\theta = 0.425$, with an increase of 44%, but afterward showed a decreasing trend up to $\theta = 0.825$, with a decrease of 34% relative to the value at $\theta = 0.425$ (fig. C1A). This meant that overall, SD for T at $\theta = 0.825$ was very similar to the initial value at $\theta = 0.1$ (0.00742 vs. 0.00778). To better understand the mechanisms involved in the decreasing trend in SD from $\theta = 0.425$ to 0.825, the deterministic dynamics of T around equilibria at these two θ values can be examined using the equation

$$\xi_T(t) = E_{21} \exp(\lambda_1 t) + E_{22} \exp(\lambda_2 t) + E_{23} \exp(\lambda_3 t), \quad (C1)$$

where $\xi_T = T - \bar{T}$, with \bar{T} being an equilibrium value of T at a particular θ value; λ_1 , λ_2 , and λ_3 are the three eigenvalues of the system for a particular θ value; and E_{21} , E_{22} , and E_{23} are constants, which also depend on θ . As θ increases from 0.425 to 0.825, the three eigenvalues remain negative, but $\lambda_3 \rightarrow 0$, so long-term dynamics become dominated by the third term in equation (C1). Thus, given a fixed initial point close to equilibrium, long-term dynamics become further away from equilibrium as θ approaches the critical threshold. However, in the short term, the first two terms in equation (C1) are not negligible compared with the third; in fact, the second term has a relatively large negative constant (E_{22}) that has a large effect in decreasing $\xi_T(t)$, as shown in figure C1B. Thus, in the short term, the net effect of the three terms in equation (C1) could result in dynamics that are closer to equilibrium as θ approaches the critical threshold; an example is shown in figure C1B for $t \leq 5$ years. For stochastic dynamics, this could lead to decreasing SD approaching the threshold if stochastic fluctuations occur frequently enough for deterministic dynamics in between the fluctuations to approximate short-term deterministic dynamics. Interestingly, short-term dynamics being closer to equilibrium nearer the critical θ value can also be demonstrated for M , using the analogous equation

$$\xi_M(t) = E_{31} \exp(\lambda_1 t) + E_{32} \exp(\lambda_2 t) + E_{33} \exp(\lambda_3 t), \quad (C2)$$

as shown in figure C1B for $3 \leq t \leq 6$ years. However, in contrast to the SD of T , the SD of M increases approaching the critical threshold of θ (fig. C1A). A possible explanation for this apparent paradox is that the dynamics of M are less frequently affected by stochastic fluctuations, as a result of the growth rate of and grazing rate on macroalgae being an order of magnitude lower than for turf algae (app. B), such that deterministic dynamics in between the fluctuations are closer to the long-term dynamics.

A derivation of equations (C1) and (C2) is now presented, together with explicit formulas for the constants. Near an equilibrium of the dynamical coral reef benthic system defined by equations (1)–(3), $(\bar{C}, \bar{T}, \bar{M})$, linearization using Taylor’s theorem shows that system dynamics can be described by

$$\mathbf{x}(t) = A_1 \exp(\lambda_1 t) \mathbf{v}_1 + A_2 \exp(\lambda_2 t) \mathbf{v}_2 + A_3 \exp(\lambda_3 t) \mathbf{v}_3, \quad (C3)$$

where $\mathbf{x}(t) = (\xi_C(t), \xi_T(t), \xi_M(t))$ is the vector of proportional covers relative to $(\bar{C}, \bar{T}, \bar{M})$, $\{\lambda_i\}_{i=1}^3$ are the eigenvalues of the interaction matrix for the linearized system, and $\{\mathbf{v}_i = (v_{i,1}, v_{i,2}, v_{i,3})\}_{i=1}^3$ are the corresponding eigenvectors. At $t = 0$, equation (C3) gives three equations that can be simultaneously solved for the constants $\{A_i\}_{i=1}^3$:

$$\xi_{C0} = A_1 v_{1,1} + A_2 v_{2,1} + A_3 v_{3,1}, \quad (C4a)$$

$$\xi_{T0} = A_1 v_{1,2} + A_2 v_{2,2} + A_3 v_{3,2}, \quad (C4b)$$

$$\xi_{M0} = A_1 v_{1,3} + A_2 v_{2,3} + A_3 v_{3,3}, \quad (C4c)$$

where $\xi_c(0) = \xi_{c0}$, $\xi_T(0) = \xi_{T0}$, and $\xi_M(0) = \xi_{M0}$. From equation (C4a),

$$A_1 = \frac{\xi_{c0} - A_2 v_{2,1} - A_3 v_{3,1}}{v_{1,1}}. \quad (C5)$$

Substituting equation (C5) into equations (C4b) and (C4c) and solving for A_2 gives

$$A_2 = \left(\frac{\xi_{T0} v_{1,1} - \xi_{c0} v_{1,2}}{v_{1,1} v_{2,2} - v_{1,2} v_{2,1}} \right) - A_3 \left(\frac{v_{1,1} v_{3,2} - v_{1,2} v_{3,1}}{v_{1,1} v_{2,2} - v_{1,2} v_{2,1}} \right). \quad (C6)$$

Substituting equations (C5) and (C6) into equation (C4c) and solving for A_3 gives

$$A_3 = \frac{(\xi_{M0} v_{1,1} - \xi_{c0} v_{1,3})(v_{1,1} v_{2,2} - v_{1,2} v_{2,1}) - (\xi_{T0} v_{1,1} - \xi_{c0} v_{1,2})(v_{1,1} v_{2,3} - v_{1,3} v_{2,1})}{(v_{1,1} v_{3,3} - v_{1,3} v_{3,1})(v_{1,1} v_{2,2} - v_{1,2} v_{2,1}) - (v_{1,1} v_{3,2} - v_{1,2} v_{3,1})(v_{1,1} v_{2,3} - v_{1,3} v_{2,1})}. \quad (C7)$$

Substituting equation (C7) into equation (C6) eliminates A_3 ; substituting equations (C6) and (C7) into equation (C5) eliminates A_2 and A_3 . Equation (C3) can then be written as:

$$\xi_c(t) = E_{11} \exp(\lambda_1 t) + E_{12} \exp(\lambda_2 t) + E_{13} \exp(\lambda_3 t), \quad (C8a)$$

$$\xi_T(t) = E_{21} \exp(\lambda_1 t) + E_{22} \exp(\lambda_2 t) + E_{23} \exp(\lambda_3 t), \quad (C8b)$$

$$\xi_M(t) = E_{31} \exp(\lambda_1 t) + E_{32} \exp(\lambda_2 t) + E_{33} \exp(\lambda_3 t), \quad (C8c)$$

where $E_{ij} = A_j v_{j,i}$, with the constants $\{A_i\}_{i=1}^3$ given explicitly by equations (C5), (C6), and (C7). Equations (C8b) and (C8c) are equivalent to equations (C1) and (C2), respectively.

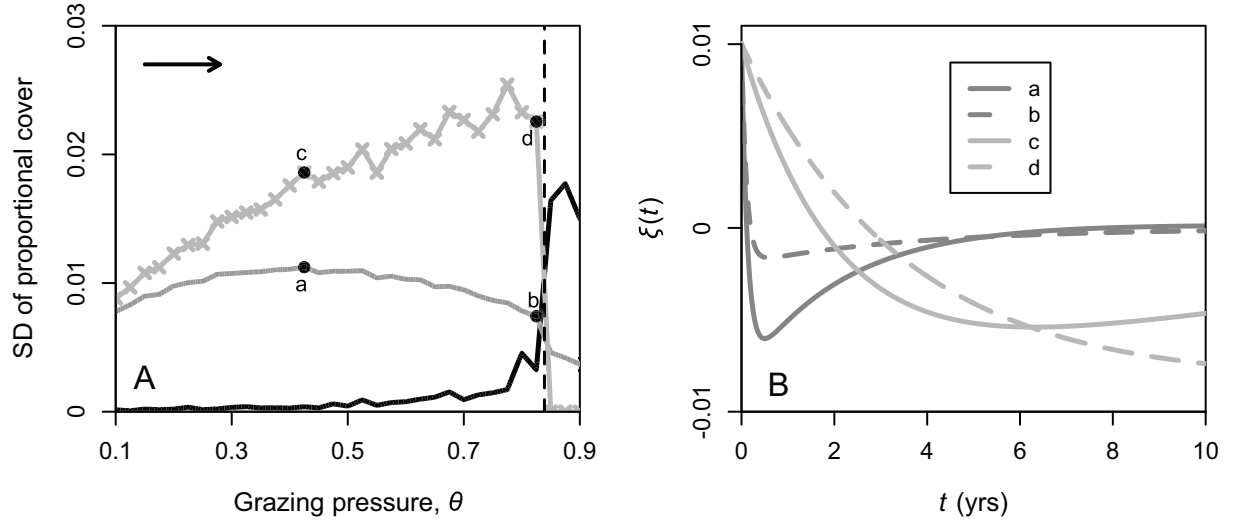


Figure C1: A, For the stochastic coral reef benthic model with 1,000 discrete units, trends in standard deviation (SD) of stationary distributions of model variables as the grazing pressure θ increases from 0.1 to 0.9 in increments of 0.025 past the critical threshold represented by the dashed vertical line. The arrow indicates the direction of θ change. Black, dark gray, and light gray lines correspond to the proportional covers of corals, turf algae, and macroalgae, respectively. Crosses on the light gray lines indicate the values of θ simulated. The parameter set used is the same as that used to draw the phase diagram in figure 1B. B, For $\theta = 0.425$ and 0.825 , corresponding to the solid and dashed lines, respectively, time dynamics for the corresponding deterministic model close to equilibrium. Starting from an initial value of 0.01, the dark gray and light gray lines show dynamics for turf algal and macroalgal proportional covers relative to the equilibrium, respectively, given by equations (C1) and (C2), respectively. The lines are labeled a–d; for each line, the SD for the corresponding stochastic model dynamics is also indicated by labels a–d in A (a: $\theta = 0.425$, turf algal cover; b: $\theta = 0.825$, turf algal cover; c: $\theta = 0.425$, macroalgal cover; d: $\theta = 0.825$, macroalgal cover).

Appendix D from T. Fung et al., “Warning Signals of Regime Shifts as Intrinsic Properties of Endogenous Dynamics”

(Am. Nat., vol. 182, no. 2, p. 208)

Results Showing Trends in Standard Deviation and Skewness for 10,000 Discrete Benthic Units, Stochastic Variation in Length of Period of Attraction by a Saddle Point, and a Regime Shift Reversal for a Model Coral Reef Undergoing Nutrient Enrichment

Trends in Standard Deviation and Skewness for 10,000 Discrete Benthic Units

Figure 2 shows trends in standard deviation (SD) and skewness for stationary dynamics as grazing pressure θ decreases from 0.9 to a critical threshold at 0.312 and as θ increases from 0.1 to another critical threshold at 0.426. The parameter values used are the same as those used to draw the phase diagram in figure 1A, and 1,000 discrete benthic units were used in the stochastic model. Figure D1 is the same as figure 2, except that 10,000 discrete benthic units were used instead. For both decreasing and increasing θ , the same increasing trends for SD and lack of clear trends for skewness were found, using 10,000 units as for 1,000 units. For each of the three variables and for decreasing or increasing θ , SD values using 10,000 units were highly correlated with those derived using 1,000 units, with $r^2 > 0.976$ ($n = 33$).

Stochastic Variation in Length of Period of Attraction by a Saddle Point

Figure 4A shows stochastic time dynamics for a simulation using the parameter set corresponding to the phase diagram in figure 1A. θ is set to 0.7 for the first 1,000 years; at 1,000 years, θ is set to 0.3, and macroalgal cover M is increased from 0 to 0.01, initiating a regime shift. During this regime shift, transient dynamics were attracted to an unstable saddle point, most clearly seen as a temporary period of stability at an intermediate coral proportional cover. Figure D2 shows how this temporary period of stability varies in length when two other simulations are performed with different seeds for the random number generator and compares the stochastic trajectories with the deterministic trajectory. It shows that in the stochastic simulations, the period of stability can be longer or shorter than for the deterministic case.

A Regime Shift Reversal for a Model Coral Reef Undergoing Nutrient Enrichment

Figure 4B shows that attraction by an unstable saddle point during a regime shift can allow a coral-algal regime shift to be reversed, if θ is increased back to a precritical value. This reversal can also be demonstrated for the case of increasing nutrient enrichment, or nitrification (sensu Szmant 2002), as shown in figure D3; this figure uses a parameter set corresponding to the one used to draw the phase diagram shown in figure 4C of Fung et al. (2011), which is reproduced in appendix B. The nutrient level is low for the first 1,000 years but is then increased past a critical threshold for 200 years, with macroalgal cover M increased from 0 to 0.01 at the threshold (increasing M is necessary to initiate a regime shift, as for the simulation in figure 4B); a discontinuous regime shift is initiated at the threshold. However, if the nutrient level is decreased to just below the critical threshold at 1,200 years, then the regime shift is reversed. Thus, hysteresis in the system is avoided. Increases and decreases in the nutrient level are modeled indirectly as increases and decreases in the growth rates of turf algae and macroalgae.

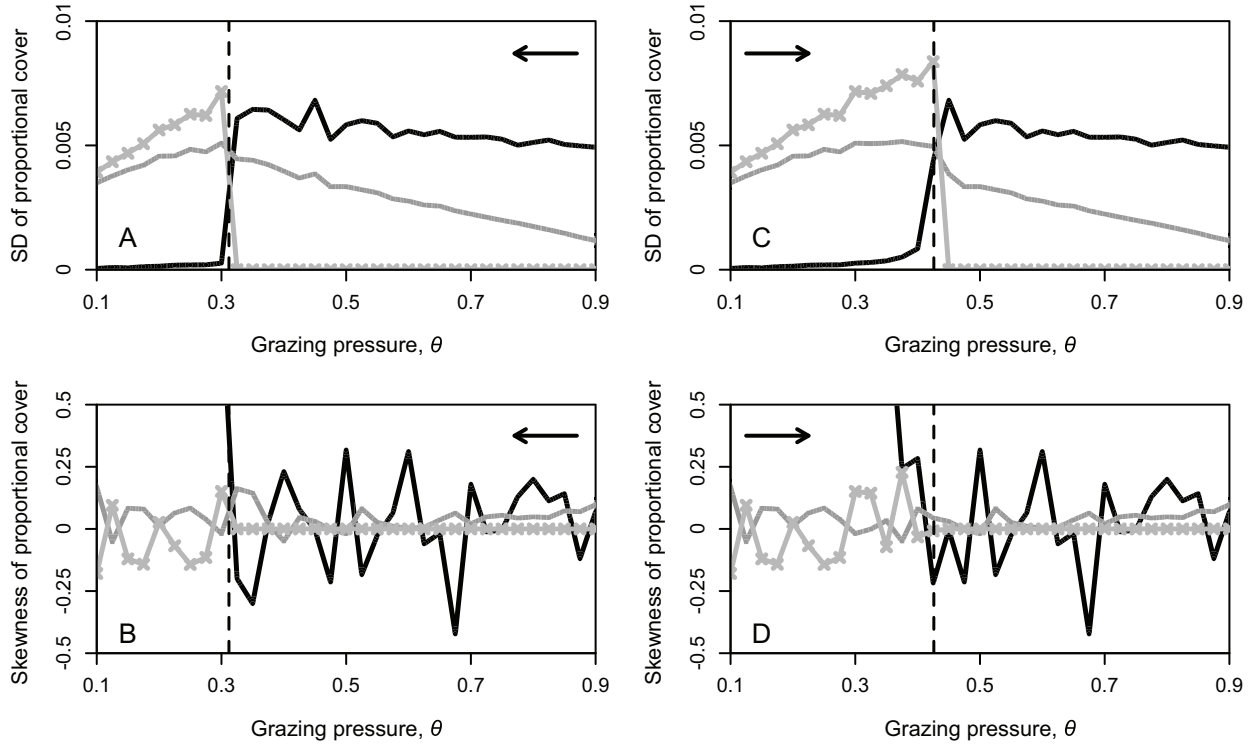


Figure D1: *A, B*, For the stochastic coral reef benthic model with 10,000 discrete units, trends in standard deviation (SD) and skewness of stationary distributions of model variables as the grazing pressure θ decreases from 0.9 to 0.1 in increments of 0.025. Same as figure 2, except that 10,000 discrete benthic units were used instead of 1,000. Black, dark gray, and light gray lines correspond to the proportional covers of corals, turf algae, and macroalgae, respectively. Crosses on the light gray lines indicate the values of θ simulated. For macroalgal cover, skewness is set to 0 if the mean is 0. The dashed vertical lines represent the critical θ value, whereas arrows indicate the direction of changing θ . The parameter set used is the same as that used to draw the phase diagram in figure 1A. *C, D*, Same as *A* and *B*, respectively, except for the case where θ increases from 0.1 to 0.9.

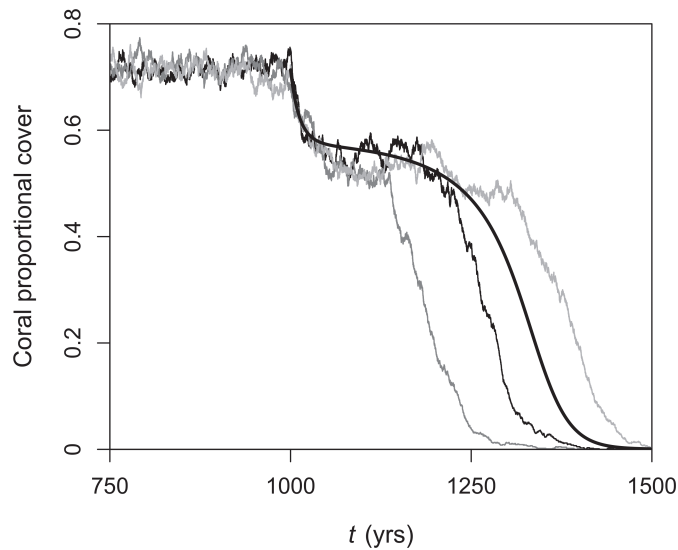


Figure D2: Three stochastic coral reef benthic model runs (fluctuating black, dark gray, and light gray lines) with the parameter set used to draw the phase diagram in figure 1A and grazing pressure parameter $\theta = 0.7$ for the first 1,000 years. One thousand discrete benthic units were used. At 1,000 years, θ is decreased to 0.3, and macroalgal proportional cover is increased from 0 by 0.01 to simulate a

macroalgal recruitment event. This causes a regime shift to low coral cover. Because of stochasticity, the length of time for which coral proportional cover remains between 0.4 and 0.6 at the intermediate step as a result of attraction by an unstable saddle point varies by more than a factor of 2. For comparison, the trajectory from the corresponding deterministic model (smooth black line) is shown as well.

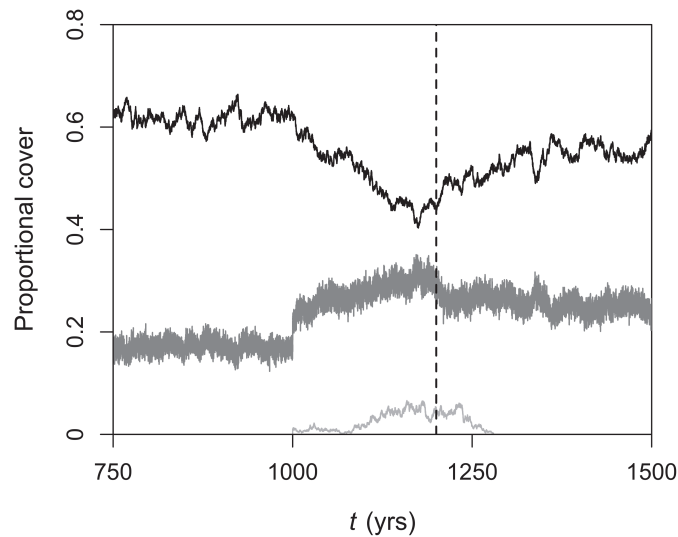


Figure D3: Stochastic coral reef benthic model run with the parameter set used to draw figure 4C of Fung et al. (2011) and turf algal and macroalgal growth rates of 11 and 0.35 year⁻¹, respectively, for the first 1,000 years. These parameter values correspond to a pristine reef with no eutrophication (Fung et al. 2011). One thousand discrete benthic units were used. Black, dark gray, and light gray lines correspond to coral, turf algal, and macroalgal covers, respectively; the initial values of these three types of cover are 0.6, 0.1, and 0.1, respectively. At 1,000 years, the turf algal and macroalgal growth rates are increased by 77% to 19.5 and 0.62 year⁻¹, respectively, representing eutrophication, and macroalgal proportional cover is increased from 0 by 0.01 to simulate a macroalgal recruitment event. This initiates a regime shift to low coral cover. If there are no further changes in algal growth rates, coral cover eventually drops to a very low value; however, in this simulation, during the regime shift at 1,200 years, the turf algal and macroalgal growth rates are decreased by 11% to 17.3 and 0.55 year⁻¹, respectively, which reverses the decline in coral cover.

Literature Cited in Appendix D

- Fung, T., R. M. Seymour, and C. R. Johnson. 2011. Alternative stable states and phase shifts in coral reefs under anthropogenic stress. *Ecology* 92:967–982.
- Szmant, A. M. 2002. Nutrient enrichment on coral reefs: is it a major cause of coral reef decline? *Estuaries* 25:743–766.

Appendix E from T. Fung et al., “Warning Signals of Regime Shifts as Intrinsic Properties of Endogenous Dynamics”

(Am. Nat., vol. 182, no. 2, p. 208)

A Spatial Extension of the Stochastic Coral Reef Model with Preliminary Results on Early Warning Signals

The nonspatial stochastic coral reef model with $N = 1,000$ discrete benthic units is extended by arranging the units in a rectangular grid with 25 rows and 40 columns (25 and 40 is the pair of integers minimizing the difference in row and column numbers). A unit is considered a neighbor of another if it is horizontally, vertically, or diagonally adjacent (i.e., the Moore neighborhood is considered). In each discrete time step, overgrowth interactions are assumed to occur only between neighboring units. Also, recruitment of brooding corals is assumed to occur only on neighboring units of space or turf algae, because there is evidence that their larvae have very short dispersal distances of centimeters (Jackson 1986; Richmond 1997). These spatially constrained processes mean that, unlike the nonspatial model, the state transition probabilities can differ between units. Specifically, for a unit in row m and column n (the focal unit), the probabilities of elementary events $e2$, $e7$, and $e13$ (for definitions of all elementary events, see app. A) are now $\gamma_{CM}r_M M_{mn}\delta t$, $\gamma_{TM}r_M M_{mn}\delta t$, and $r_M M_{mn}\delta t$, respectively, where

$$M_{mn} = \frac{\sum_{a=1}^{25} \sum_{b=1}^{40} w_{mn,ab} y_{ab}}{\sum_{a=1}^{25} \sum_{b=1}^{40} w_{mn,ab}}. \quad (E1)$$

Here, $w_{mn,ab} = 1$ if the unit in row a and column b is a neighbor of the focal unit and 0 otherwise, and $y_{ab} = 1$ if the unit in row a and column b is occupied by macroalgae (i.e., is in state 2) and 0 otherwise. This expression arises because only macroalgal units in the neighborhood of the focal unit are considered. Similarly, the probabilities of $e4$ and $e10$ are now $\varepsilon_C l_C^b C_{mn} \delta t$ and $l_C^b C_{mn} \delta t$, respectively, where

$$C_{mn} = \frac{\sum_{a=1}^{25} \sum_{b=1}^{40} w_{mn,ab} z_{ab}}{\sum_{a=1}^{25} \sum_{b=1}^{40} w_{mn,ab}}, \quad (E2)$$

with $z_{ab} = 1$ if the unit in row a and column b is occupied by corals (i.e., is in state 0) and 0 otherwise.

The probabilities of $e5$ and $e11$ —representing overgrowth of corals over a focal turf algal and space unit, respectively—also change but in a more complicated way because there is a need to consider the neighborhood of each coral neighbor to see how many macroalgal units are constraining its growth. These probabilities are now given by

$$\frac{\sum_{a=1}^{25} \sum_{b=1}^{40} w_{mn,ab} z_{ab} [\alpha_C r_C (1 - \beta_M M_{ab}) \delta t]}{\sum_{a=1}^{25} \sum_{b=1}^{40} w_{mn,ab}}, \quad (E3)$$

$$\frac{\sum_{a=1}^{25} \sum_{b=1}^{40} w_{mn,ab} z_{ab} [r_C (1 - \beta_M M_{ab}) \delta t]}{\sum_{a=1}^{25} \sum_{b=1}^{40} w_{mn,ab}}, \quad (E4)$$

respectively. Transition probabilities for the remaining elementary events remain the same as for the nonspatial model, since they do not depend on spatially constrained processes.

For grazing pressure $\theta = 0.9$ and all other parameters set to values used to draw figure 1A, the spatial stochastic coral reef model is run for 2,000 years, with a time step of $\delta t = 1$ day. Initially, there are 600, 100, and 100 units of coral, turf algae, and macroalgae, respectively, randomly distributed among the rectangular grid. This gives initial values of 0.6, 0.1, and 0.1 for the corresponding proportional covers C , T , and M , respectively. After 500 years, there is convergence to a stationary state (determined by visual inspection), and the subsequent 1,500 years of data are used to calculate the mean, standard deviation (SD), and skewness for the stationary distributions of C , T , and M . This exercise is repeated for $\theta = 0.875$ down to 0.1 in increments of 0.025. For $\theta = 0.325$, initially, 800, 100, and 50 units of coral, turf algae, and macroalgae, respectively, are used to achieve convergence after 500 years. Similarly, for $\theta = 0.3$, the initial numbers of

units of coral, turf algae, and macroalgae used are 100, 100, and 600, respectively. Before the critical value of $\theta_c^- = 0.312$ is reached, there is always convergence to a stationary state with high (>0.5) mean C .

Across the θ values tested, for C , T , or M , the spatial model produced stationary distributions with means that are highly correlated with those from the nonspatial model ($r^2 > 0.997$, $n = 33$), with the regression lines having y-intercepts close to 0 (magnitude <0.003) and slopes close to 1 (<0.101 away from 1). Furthermore, as θ decreases to $\theta_c^- = 0.312$, SD for C and T showed an increasing trend, whereas skewness for C fluctuated wildly with no clear trend and skewness for T decreased (fig. E1). These trends are the same as those for the nonspatial model (fig. 2A, 2B); in fact, across all θ values tested, for C , T , or M , SD values derived using the spatial model are highly correlated with those from the nonspatial model ($r^2 > 0.932$, $n = 33$), with the regression lines having y-intercepts close to 0 (magnitude <0.0007) and slopes close to 1 (<0.135 away from 1).

In future work, the sensitivity of the preliminary results presented here to changes in assumptions underlying the spatial model can be tested. For example, simulations can be performed with a spatial model that has a different spatial configuration, a different number of benthic units, and/or periodic boundaries.

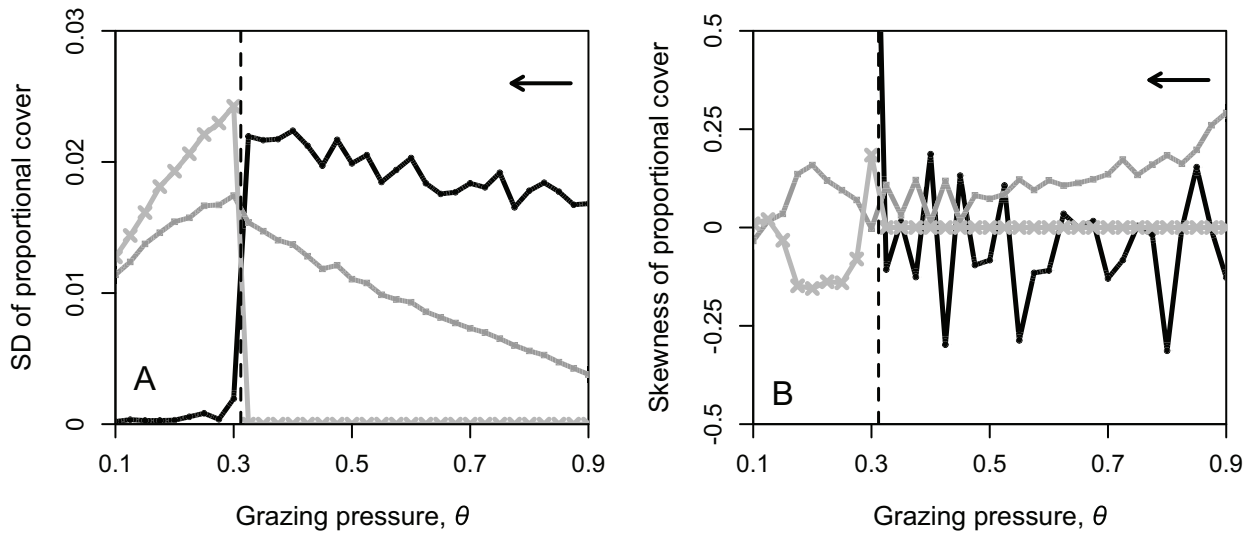


Figure E1: A, B, For the spatially extended stochastic coral reef benthic model, trends in standard deviation (SD) and skewness of stationary distributions of model variables as the grazing pressure θ is decreased. Black, dark gray, and light gray lines correspond to the proportional covers of corals, turf algae, and macroalgae, respectively. Crosses on the light gray lines indicate the values of θ simulated. For macroalgal cover, skewness is set to 0 if the mean is 0. The dashed vertical lines represent the critical θ value, whereas arrows indicate the direction of changing θ .

Literature Cited in Appendix E

- Jackson, J. B. C. 1986. Modes of dispersal of clonal benthic invertebrates: consequences for species' distributions and genetic structure of local populations. *Bulletin of Marine Science* 39:588–606.
- Richmond, R. H. 1997. Reproduction and recruitment in corals: critical links in the persistence of reefs. Pages 175–197 in C. Birkeland, ed. *Life and death of coral reefs*. Chapman & Hall, New York.